Geophysical Journal International

Geophys. J. Int. (2013) **193,** 1053–1070
Advance Access publication 2013 March 26

doi: 10.1093/gji/ggs114

Microseismicity and seismotectonics of the South Caspian Lowlands, NE Iran

Majid Nemati,[1,2] James Hollingsworth,[3] Zhongwen Zhan,[4] Mohammad Javad Bolourchi[2] and Morteza Talebian[2]

[1] *Shahid Bahonar University of Kerman, Science faculty, Geology department, PO Box* 76169133, *Kerman, Iran. E-mail: majid_1974@uk.ac.ir*
[2] *Geological Survey of Iran, PO Box* 13185–1494, *Tehran, Iran*
[3] *Géoazur, University of Nice Sophia-Antipolis, CNRS, Observatoire de la Côte d'Azur,* 250 *rue Albert Einstein, Sophia Antipolis* 06560 *Valbonne, France*
[4] *Division of GPS, California Institute of Technology, MC* 100-23, *Pasadena, CA* 91125, *USA*

Accepted 2012 December 18. Received 2012 December 17; in original form 2012 January 24

SUMMARY

This paper is concerned with the microseismicity and seismotectonics of the eastern South Caspian Sea region, where the East Alborz mountains descend to meet the South Caspian Lowlands of NE Iran. To better understand the present-day tectonics and seismicity of this region, which includes the cities of Gorgan and Gonbad-e-Qabus (combined population 500 000), we installed a temporary local seismic network across the area for 6 months between 2009 and 2010. We analysed the seismicity and focal mechanisms together with data from the permanent networks of the Institute of Geophysics, University of Tehran (IGUT) and the International Institute of Earthquake Engineering and Seismology (IIEES), based in Tehran. Microseismicity is focused primarily on the Shahrud fault system, which bounds the east Alborz range to the south. Relatively few earthquakes are associated with the Khazar thrust fault, which bounds the north side of the range. A cluster of shallow microseismicity (<15 km depth) occurs 40 km north of the Khazar fault (within the South Caspian Lowlands; SCL), an area typically thought to be non-deforming. This area coincides with the location of three relatively deep thrust earthquakes (M_w 5.3–5.5) which occurred in 1999, 2004 and 2005. Inversion of teleseismic body waveforms allows us to constrain the depth of these earthquakes at 26–29 km. Although significant sedimentation throughout the SCL obscures any expression of recent fault activity at the surface, focal mechanisms of well-located events from the shallow cluster of micro-seismicity show a significant component of left-lateral strike-slip motion (assuming slip occurs on NE–SW fault planes, typical of active faults in the region), as well as a small normal component. Inversion of traveltimes for well-located events in our network yields a velocity structure for the region, and a Moho depth of 41 km. The pattern of deep thrust and shallow normal seismicity could be explained by bending of the rigid South Caspian crust as it underthrusts the East Alborz mountains and Central Iran. Late Quaternary reorganization of drainage systems in the SCL may be the result of shallow normal fault activity within the SCL.

Key words: Earthquake source observations; Seismicity and tectonics; Continental neotectonics; Tectonics and landscape evolution; Crustal structure; Asia.

1 INTRODUCTION

Iran is currently deforming as a result of the northward collision of Arabia with Eurasia. Despite a relatively good understanding of how the broad-scale deformation is currently accommodated throughout this wide (>1000 km) region (e.g. Berberian 1981; Jackson & McKenzie 1984; Jackson *et al.* 1995; Axen *et al.* 2001; Jackson *et al.* 2002; Vernant *et al.* 2004b; Walker & Jackson 2004; Allen *et al.* 2006; Copley & Jackson 2006; Talebian *et al.* 2006; Walpersdorf *et al.* 2006; Djamour *et al.* 2010; Hollingsworth *et al.* 2010a; Allen *et al.* 2011; Nissen *et al.* 2011), the detailed tectonics of many earthquake-prone regions throughout the country still remain poorly understood. This study focuses on the South Caspian Lowlands (SCL), a unique area in NE Iran which forms the southern margin of the relatively non-deforming, aseismic South Caspian block, yet also lies between the deforming Kopeh Dagh and Alborz mountains to the east and south, respectively. The SCL and neighbouring areas have experienced many destructive earthquakes over the past few centuries (Fig. 1), which highlight their importance in accommodating regional shortening (Tchalenko 1975; Berberian

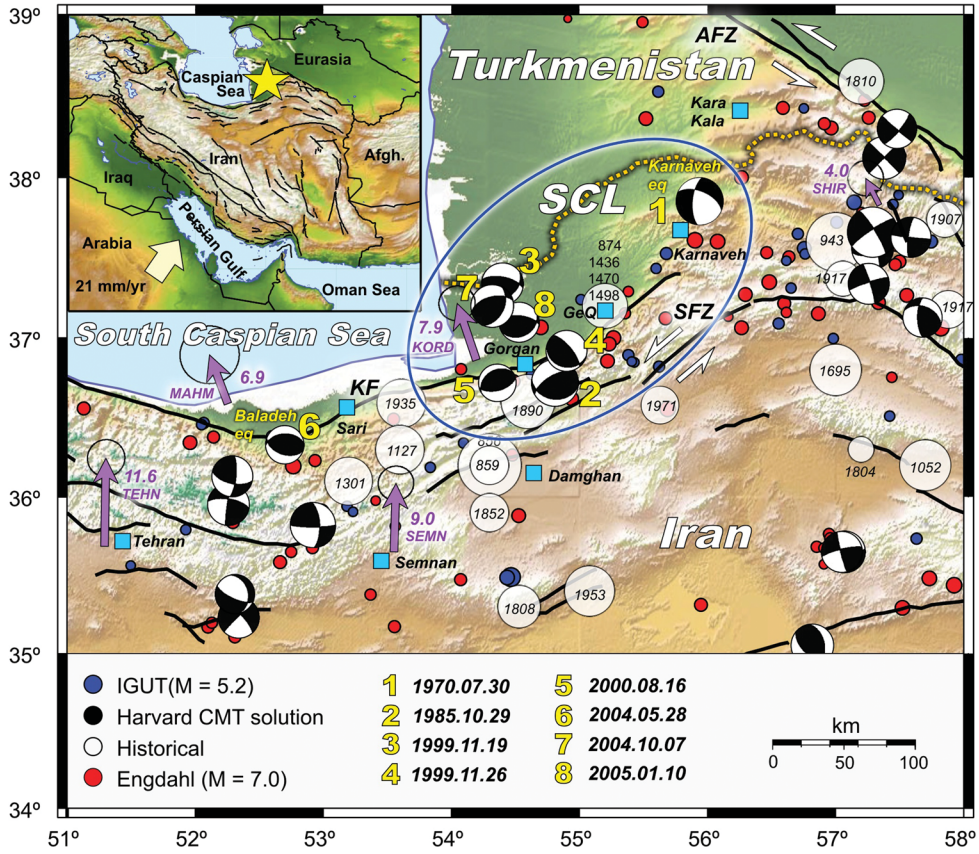

Figure 1. Summary topographic map of NE Iran corresponding to the yellow star in the inset figure. Historical and instrumental seismicity for the Central and East Alborz, West Kopeh Dagh and South Caspian Lowland (SCL) are shown: historical earthquakes (white circles) are from Ambraseys & Melville (1982), black focal mechanisms are from the Global CMT catalogue, red circles are epicentres from the catalogue of Engdahl *et al.* (2006), blue circles are epicentres recorded by the Institute of Geophysics, University of Tehran (IGUT) seismic network ($M_N > 4.0$). The 1970 Karnaveh and 2004 Baladeh earthquakes are labelled in yellow. Yellow numbers show the dates for various earthquakes in the SCL region. Blue squares show major cities across the region; GeQ, Gonbad-e-Qabus. Black lines show various faults. Blue ellipse highlights the SCL region, which is the focus of this study.

& King 1981; Ambraseys & Melville 1982; Jackson *et al.* 2002; Hollingsworth *et al.* 2006; Shabanian *et al.* 2009b). The primary aim of this paper is to better understand the role of the SCL within the wider Arabia–Eurasia collision zone. Furthermore, with a combined population of >500 000 people in the cities of Gorgan and Gonbad-e-Qabus (Fig. 1), plus many more living in neighbouring towns and villages, and a regionally important power plant at Neka, any attempt to improve our understanding of the seismic hazard posed to this area by active faults is of fundamental importance.

Due to the relative lack of seismicity in the SCL, and very few geological outcrops across the region, a seismological study was undertaken to help clarify the subsurface tectonics. We investigated the microseismicity of the SCL region during a 6-month period (spanning 2009–2010) using a network of 10 medium band CMG-3ESP Güralp instruments, owned by the Geological Survey of Iran. This data was combined with 4 yr of seismicity data recorded by seismic networks of the Institute of Geophysics, University of Tehran (IGUT) and the International Institute of Earthquake Engineering and Seismology (IIEES) of Iran. Because the seismic moment release from micro-earthquakes is relatively small compared with larger earthquakes ($M_w > 5.2$), and they rupture small fault areas away from the major fault structures, they may not always provide a representative picture of the active tectonics for a region. The approach used in this study is to combine data from local and teleseismic seismicity, the crustal structure and tectonic geomorphology so we can provide a coherent picture of the active tectonics of the SCL region of NE Iran; where information from any one of those data sources alone might be ambiguous and inconclusive.

2 TECTONIC SETTING AND SEISMICITY

The 3000 m high Alborz mountains of Northern Iran have formed in successive tectonic events related to the collision of Central Iran with Eurasia in the Late Triassic (Cimmerian Orogeny) and the present-day collision of Arabia with Eurasia (Berberian & King 1981; Alavi 1996; Zanchi *et al.* 2006). Immediately north of the Alborz lie the SCL, which form a low lying area around the edge of the South Caspian Basin (SCB). This region is notable for its thick sedimentary deposits, which yield significant volumes of oil and gas (Devlin *et al.* 1999; Brunet *et al.* 2003). The SCB is bordered to the south and west by major thrust belts of the Alborz, Talysh and Kopeh Dagh, and to the north by a young subduction zone, the Apsheron-Balkhan Sill (Jackson *et al.* 2002). The Alborz mountains bound the SCB to the south, forming a boundary separating rocks with a Central Iran affinity from rocks with Eurasian origins (Stöcklin 1974). The SCB contains up to 20 km of sedimentary deposits, making it one of the deepest sedimentary basins in

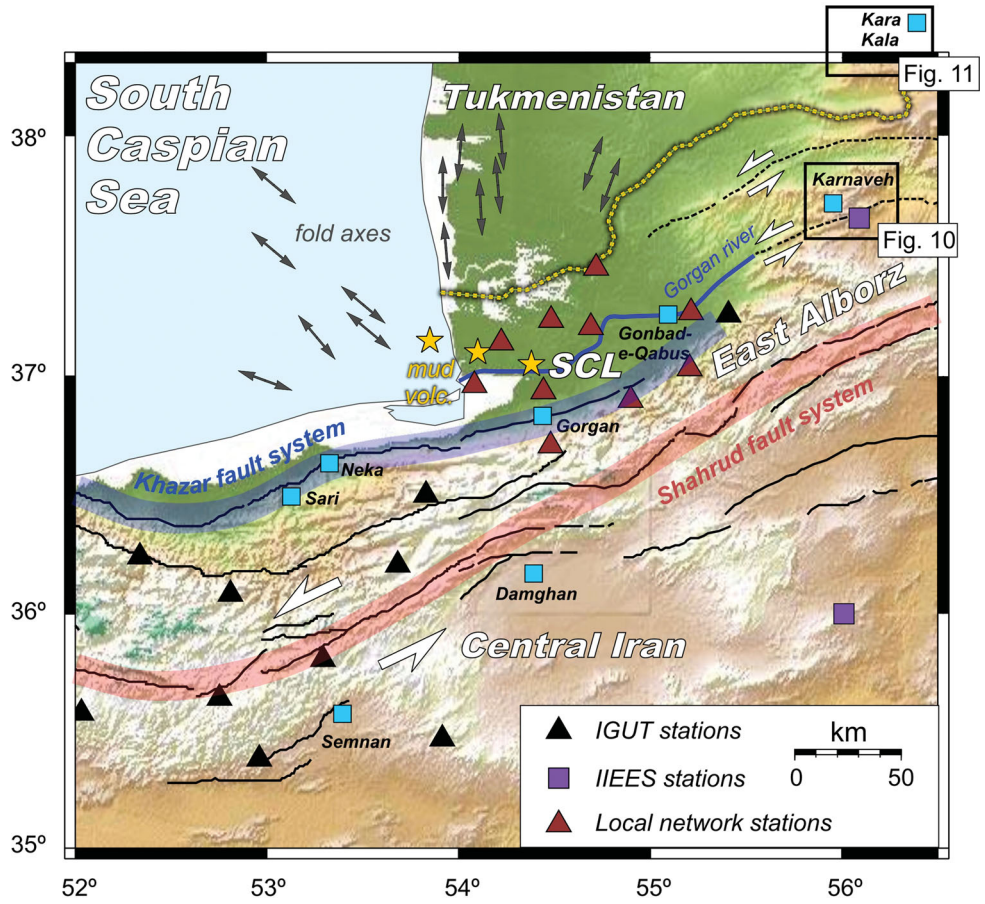

Figure 2. Map showing the location of both permanent and temporary seismic networks used in this study. Black triangles are IGUT stations, purple squares are from the IIEES network, and red triangles are from our temporary network. Orange stars show mud volcanoes (Ansari & Bolourchi 2003) in the SCL region, which highlight the ductile nature of thick and shallow sedimentary sequences characteristic of this foreland basin setting. Thin blue line shows the Gorgan river. Grey arrows show the direction of fold axes, adapted from Hinds *et al.* (2007). The Khazar thrust fault is highlighted by a thick blue line; the Shahrud fault system is highlighted by a thick red line.

the word (Brunet *et al.* 2003). A stratigraphic column for the western SCB suggests about 2.4 km of subsidence has occurred since 5.5 Ma (Allen *et al.* 2002). Rapid rates of deposition within the basin during this time has generated overpressure via disequilibrium compaction, leading to the formation of mud volcanoes throughout the South Caspian area (Fig. 2, Kopf *et al.* 2001; Yusifov & Rabinowitz 2004; Stewart & Davies 2006). The thick sediments of the SCB overlie a high velocity basement that is thinner within the basin, and thicker around its margins (Mangino & Priestley 1998). The basement beneath the basin could either be unusually thick oceanic crust or thinned, high velocity continental crust (e.g. Berberian & King 1981; Kadinsky-Cade *et al.* 1981; Jackson *et al.* 2002). A lack of earthquakes within the basin indicates the SCB behaves as a relatively non-deforming rigid block caught up within the wider Arabia–Eurasia collision zone. Nevertheless, significant folding of the sedimentary cover has resulted in the formation of many hydrocarbon reservoirs within the basin (Devlin *et al.* 1999; Knapp *et al.* 2004).

Despite the clear expression of active faults within the east Alborz region (Ritz *et al.* 2006; Hollingsworth *et al.* 2008, 2010b; Javidfakhr *et al.* 2011), there has been relatively little seismicity associated with these structures over the last 50 yr. The Alborz mountains are currently being thrust over the SCB by the Khazar fault, which runs along the northern edge of the range (Tatar *et al.* 2007). Although the Khazar fault is not clearly expressed in the Late Quaternary geomorphology, compared with other thrust faults in the desert regions of Iran (e.g. Fattahi *et al.* 2006; Hollingsworth *et al.* 2010a), recent slip on the central part of this fault is thought to be responsible for the 2004 Baladeh thrust earthquake (M_s 6.4, event 5 in Fig. 1, Tatar *et al.* 2007). The focal mechanism for this event indicated N–S shortening across the range, while the aftershock distribution revealed a S-dipping fault plane which projected to the surface along the Khazar fault trace, strongly suggesting a dominantly thrust-style of deformation on the Khazar fault. Although no large earthquakes have ruptured the southern range-front of the eastern Alborz in recent times, various studies have revealed active left-lateral slip along major range-parallel faults within the southern half of the range (Ritz *et al.* 2006; Hollingsworth *et al.* 2008, 2010b; Nemati *et al.* 2011). Deformation of the east Alborz mountains appears to be partitioned onto NNW-directed shortening on the Khazar thrust fault and ENE–WSW left lateral shear on the Shahrud fault system (Wellman 1966; Jackson *et al.* 2002; Hollingsworth *et al.* 2008). Using campaign GPS velocities from either side of the East Alborz range (Vernant *et al.* 2004a,b; Masson *et al.* 2007; Djamour *et al.* 2010), Hollingsworth *et al.* (2008, 2010b) estimated a left-lateral shear of ~3 mm yr^{-1} across the range (consistent with Quaternary rates of shear, see Javidfakhr *et al.* 2011 and Rizza *et al.* 2011). Reconciling seismicity data with GPS velocities

and active fault mapping, Jackson *et al.* (2002) and Hollingsworth *et al.* (2006, 2008) concluded the SCL has a westward component of motion, relative to both Central Iran and Eurasia.

The South Caspian interior and adjacent lowland areas, especially to the east (the region under investigation in this study), have experienced relatively few earthquakes both in recent times (Jackson *et al.* 2002), and historically (Ambraseys & Melville 1982)—for example, the 72-m-high pure-brick tower of Gonbad-e-Qabus, built in 1006 AD as a tomb for the sultan Qabus ibn Wushmgir remains in pristine condition. The most significant earthquake from the East Alborz region occurred within the southern East Alborz mountains 50 km south of Gorgan, where slip on the Astaneh fault resulted in the destruction of Damghan city in 856 AD (Ambraseys & Melville 1982; Hollingsworth *et al.* 2010b, and Fig. 1). Nevertheless, a large earthquake occurred ∼25 km SE of Gorgan in 1985, and three mid-sized earthquakes occurred 20–40 km north of Gorgan in 1999, 2004 and 2005 (Fig. 1).

The 1985 October 29, Gorgan earthquake (M_w 6.2) is the largest instrumentally recorded event to have occurred in the region of our local network (Fig. 1, Priestley *et al.* 1994). In the 2 months following the 1985 main shock, five aftershocks occurred (M_b 4.3–5.0, NEIC catalogue). Assuming a typical fault slip-to-length ratio of 5×10^{-5}, the approximate fault dimensions given a seismic moment of 2.18×10^{18} N m (Priestley *et al.* 1994) are ∼11 km, with 0.6 m of slip. Based on the 13 ± 5 km depth for the Gorgan earthquake (Priestley *et al.* 1994), and the 30–35° dip of the south-dipping nodal plane (Priestley *et al.* 1994), the fault plane projects to the surface along the Khazar fault, which runs along the northern edge of the East Alborz mountains (see later discussion, and Fig. 9). Assuming this earthquake ruptured the south-dipping Khazar fault, the focal mechanism of Priestley *et al.* (1994) indicates NNW-directed shortening, perpendicular to the Alborz range-front, suggesting a dominantly pure-thrust style of deformation for this structure (earthquake 2 in Fig. 1).

The 1999, 2004 and 2005 events are notable for being relatively deep (∼30 km; e.g. Global CMT and hypocentral relocations of Engdahl *et al.* 2006) and for their unusual location 30–50 km north of the range front within the generally aseismic SCL (Fig. 1)—most earthquakes in Iran are shallower than 20 km (e.g. Maggi *et al.* 2000; Jackson *et al.* 2002; Talebian & Jackson 2004; Nissen *et al.* 2011). Hollingsworth *et al.* (2008) suggested these deeper earthquakes may be related to flexural compression at the base of the SCL as it is underthrust beneath the Alborz, although they could also result from deep and blind thrust splays propagating north of the Alborz range front. Various kimematic models have been proposed for the region (Jackson *et al.* 2002; Hollingsworth *et al.* 2006, 2008, 2010a; Ritz *et al.* 2006; Shabanian *et al.* 2009a; Djamour *et al.* 2010; Shabanian *et al.* 2010; Javidfakhr *et al.* 2011) which show that Arabia–Eurasia shortening is accommodated by both thrust and strike-slip fault systems in the Kopeh Dagh and East Alborz ranges, with some component of westward extrusion of the Western Kopeh Dagh region between the right lateral Ashkabad fault and left-lateral Shahrud fault systems (Fig. 1). However, these models do not adequately address active deformation occurring within the SCL or West Kopeh Dagh regions, where large earthquakes such as the 1970 Karnaveh earthquake (Ambraseys *et al.* 1971) have occurred, and where recent fault movements are visible in the late Quaternary geomorphology. Northeast of Gorgan, the pattern of active faults becomes distributed, and obscured by extensive loess deposits and vegetation cover. Little is known about how faults slip in this area, and few faults have surface traces continuous over more than a few kilometres.

3 METHODS

In the following section, we first explain the various approaches we use to examine the seismicity of the SCL region using teleseismic, regional network and local network data. We then determine the velocity structure for the SCL by inverting traveltimes for well-located events in our network. The results from each analysis are outlined separately in Section 4.

3.1 Methods: teleseismic seismicity

While the 1985 Gorgan earthquake appears to have ruptured the Khazar fault (the most obvious active fault in this region), three additional earthquakes occurred in the SCL north of Gorgan between 1999 and 2005, which are less easy to associate with an active structure: 1999 November 19 (M_w 5.3, depth 30 km), 2004 October 7 (M_w 5.5, depth 32 km) and 2005 January 10 (M_w 5.4, depth 32 km)—see Figs 1 and 9. The ∼30 km depths reported by the Global CMT and Engdahl catalogues (e.g. Engdahl *et al.* 1998, 2006) for these earthquakes are unusually deep for Iran, where depths in the plateau region are typically <20 km (Maggi *et al.* 2000). Deeper earthquakes have been reported from the Trans-Caspian zone, which strikes NW–SE across the central Caspian Sea, and are thought to result from subduction of the South Caspian beneath the North Caspian Sea (part of stable Eurasia, see Jackson *et al.* 2002). Since depth estimates from the Global CMT catalogue are often poorly constrained in the shallow crust (e.g. Maggi *et al.* 2002), we use both body-waveform inversion (Zwick *et al.* 1994) and Cut-And-Paste (CAP) methods (Zhao & Helmberger 1994; Zhu & Helmberger 1996) to determine the best-fitting source parameters of these earthquakes.

We use the MT5 version (Zwick *et al.* 1994) of the McCaffrey & Abers (1988) and McCaffrey (1991) algorithm, which inverts the *P* and *SH* waveform data to obtain the strike, dip, rake, centroid depth, seismic moment and source time function of the 1999, 2004 and 2005 earthquakes. The method and approach we use are described in detail elsewhere (Nábělek 1984; McCaffrey & Nábělek 1987; Molnar & Lyon-Caen 1989; Taymaz *et al.* 1991). The CAP method first cuts teleseismic records into *P*-wave segments in the vertical components and *SH*-wave segments in the transverse components, and then fits them to synthetic waveforms independently allowing different time shifts and weights. We perform a grid-search of magnitude, depth, source duration, strike, dip and rake to find the optimal source parameters for the 2004 event with the smallest waveform misfit. Uncertainties are calculated using the bootstrapping method.

3.2 Methods: regional network seismicity

We examined 4 yr of seismicity data recorded by the regional seismic networks of the IGUT and the IIEES of Iran. The IGUT permanent network instruments are SS1 short period Nanometrics instruments each consisting of three components. The IIEES seismometers are mainly broadband Güralp CMG-3T sensors. We selected 1389 well-located events from 3941 earthquakes recorded by the IGUT network. About 4800 events were also recorded by the IIEES network between 2004 and 2010. Fig. 2 shows the locations of the IGUT and IIEES stations throughout the East Alborz region. We only consider events, which were recorded by at least four stations. To get a picture of the overall seismicity in the East Alborz and SCL region, we did not select the epicentres based on their maximum azimuthal gap. We filtered the data to include only the best-located events, thereby improving the location of the diffuse seismicity (Bondár *et al.* 2004;

Nemati *et al.* 2011). The explosions in quarries and in mines usually occur at a fixed time of the day and were removed from the data.

3.3 Methods: local network microseismicity

To better constrain the the recent microseismicity of the SCL region, a temporary network of 10 seismometers was deployed in a 100 km × 100 km region north of the city of Gorgan (Fig. 2). The instruments installed were medium-band sensors with a cut-off period of 60 s, each connected to a DM-24 digitizer. The local network was operational between 2009 October and 2010 January, while the timing of IGUT and IIEES data used in this study ranged from 2006 to 2010 and 2004 to 2010, respectively. Fig. 2 shows the location of the temporary network stations. The instruments recorded the waveform data in continuous mode, and at a sampling rate of 100 Hz. The temporary stations were visited each week for maintenance (e.g. checking of power supply and consistency of internal versus external GPS time). The appropriate horizontal amplitudes were picked to calculate a M_L equivalent Wood-Anderson magnitude. The waveforms were edited manually using the Scream software (Güralp systems LTD), and the processing was performed using the Seisan software (Havskov & Ottemöller 2005) and Hypo71 program (Lee & Lahr 1972).

3.4 Methods: velocity structure of the SCL

To better constrain the crustal structure of the SCL region, we estimated the V_p to V_s ratio from the average t_S–t_P versus t_P–t_0 of a selected set of 32 earthquakes recorded with our local network, obtaining a $V_p/V_s = 1.70$. Each earthquake was recorded by a minimum of four stations, with a maximum azimuthal gap of 180°, a maximum epicentral distance of 150 km, RMS less than 0.3 s, standard deviation of 0.03 and minimum correlation coefficient of 0.98 (Nemati *et al.* 2010).

Due to the lack of a *P*-wave velocity structure in this area, we used the shallow velocity structure of Mangino & Priestley (1998) as an initial model. We determined the crustal velocity model by inverting local traveltimes of reliable events for a 1-D velocity structure (Kissling 1988). Only events recorded with a minimum of eight phases, rms less than 0.5 s and both horizontal and vertical errors less than 5 km were used in the inversion (totaling 47 events). Because there is a non-uniqueness and correlations between the input and output models, we investigated 50 randomly distributed initial models to avoid bias in the estimated structure. The inversion process was divided into two stages. First, all the initial models consisted of 20 layers with a mean velocity of 6.0 km s^{-1} and a thickness of 2.0 km from the surface to 40 km depth, and we allowed for a maximum change of 0.5 km s^{-1} for each layer (e.g. Nemati *et al.* 2011). This allowed us to estimate the approximate depths and velocities of the real discontinuities in the velocity structure, which results in a three layer model with velocity contrasts located at 6 km, 12 km (upper crystalline layer) and 20 km depth, overlying a half-space.

4 RESULTS

4.1 Results: teleseismic seismicity

The best-fitting source parameters determined for the 1999, 2004 and 2005 earthquakes using the MT5 body-waveform modelling software are shown in Fig. 3. The best-fitting depths for each event are: 1999, 26 km; 2004, 28 km and 2005, 29 km.

The best-fitting source parameters for the 2004 earthquake, determined using the Cut-and-Paste method, are shown in Fig. 4. Figs 4(a) and (b) show the fit between the raw data and synthetic waveforms for both *P* and *SH* waves for our best-fitting source model (M_w 5.5, depth 32 km, strike 26°, dip 44°, rake 53°). Figs 4(c)–(i) show the uncertainties in our best-fitting solution. Although the rupture duration is not well constrained, we find it does not trade-off with depth (Fig. 4c), forming a well-defined minimum on the misfit curve. Although the azimuthal station distribution is not optimal, our bootstrapping error estimations give consistent results, suggesting both the focal mechanism and depth are well resolved. The best-fitting depth of 31–33 km is similar to the 28 km depth estimate determined using MT5 (Fig. 3).

4.2 Results: regional seismicity

The distribution of seismicity in the SCL for the two different regional networks used in this study is shown in Fig. 5a and b. The earthquake epicentres of the IGUT network (M_N of 0.5–4.5) were plotted from 2006 to 2010, while the epicentres of the IIEES network are from 2004 and 2010.

The majority of seismicity is focused on the left-lateral Shahrud fault system of the southern Central and East Alborz, and in the SCL north of Gorgan, in the same area as the 1999, 2004 and 2005 earthquake (Figs 1 and 5). Relatively little seismicity is associated with the Khazar fault, which strikes along the northern margin of the Alborz range, and ruptured during the 2004 Baladeh earthquake (Fig. 1, Tatar *et al.* 2007) and probably during the 1985 Gorgan earthquake (Priestley *et al.* 1994).

4.3 Results: local network seismicity

Of the 900 earthquakes (M_L range of 0.5–4.0) recorded by the temporary network, 280 events have been well-located, of which 70 are high quality, and 210 are lower quality (Fig. 6a). The depth distribution of both high and lower quality earthquakes recorded by the local network between October 2009 and January 2012 shows the majority of earthquakes occurring in the top 14 km, although earthquakes occur all the way down to the Moho at 41 km depth (Fig. 6b). Table 2 gives the nearest station distances, the number of *P* and *S* readings and azimuthal gaps used to determine the depths for each micro-earthquake.

The relatively good station covering of our local network, and also the IGUT and IIEES surrounding stations (Fig. 2), especially south of Gorgan, allows us to compute 20 first motion micro-earthquake focal mechanisms (Fig. 7 and Table 3). Based on the number of polarities, maximum rotation of the planes and polarity scattering over four quadrants, we split the focal mechanisms into two groups: black (higher quality) and grey (lower quality). In nearly all cases, the steeper NE–SW-striking nodal planes are relatively well constrained by the station coverage, compared with the NW–SE planes. The distribution of first motions and the nodal planes for each earthquake can be found in Appendix A. Depth errors are typically <5 km (Nemati *et al.* 2011). Focal mechanisms: 2, 3, 4, 5, 6, 11, 14, 16, 18, 19 and 20 have a left-lateral, and in some cases a small normal component of slip, assuming the NE–SW nodal plane represents the fault which ruptured. The mechanisms of 4 and 7 may be related to left lateral shear on fault systems in the region of Karnaveh and Kara Kala (Figs 10 and 11). Focal mechanisms 12 and 13 show a deep strike-slip (44.3 km) and thrust (40.9 km) mechanism, respectively, although both are not well constrained—nevertheless,

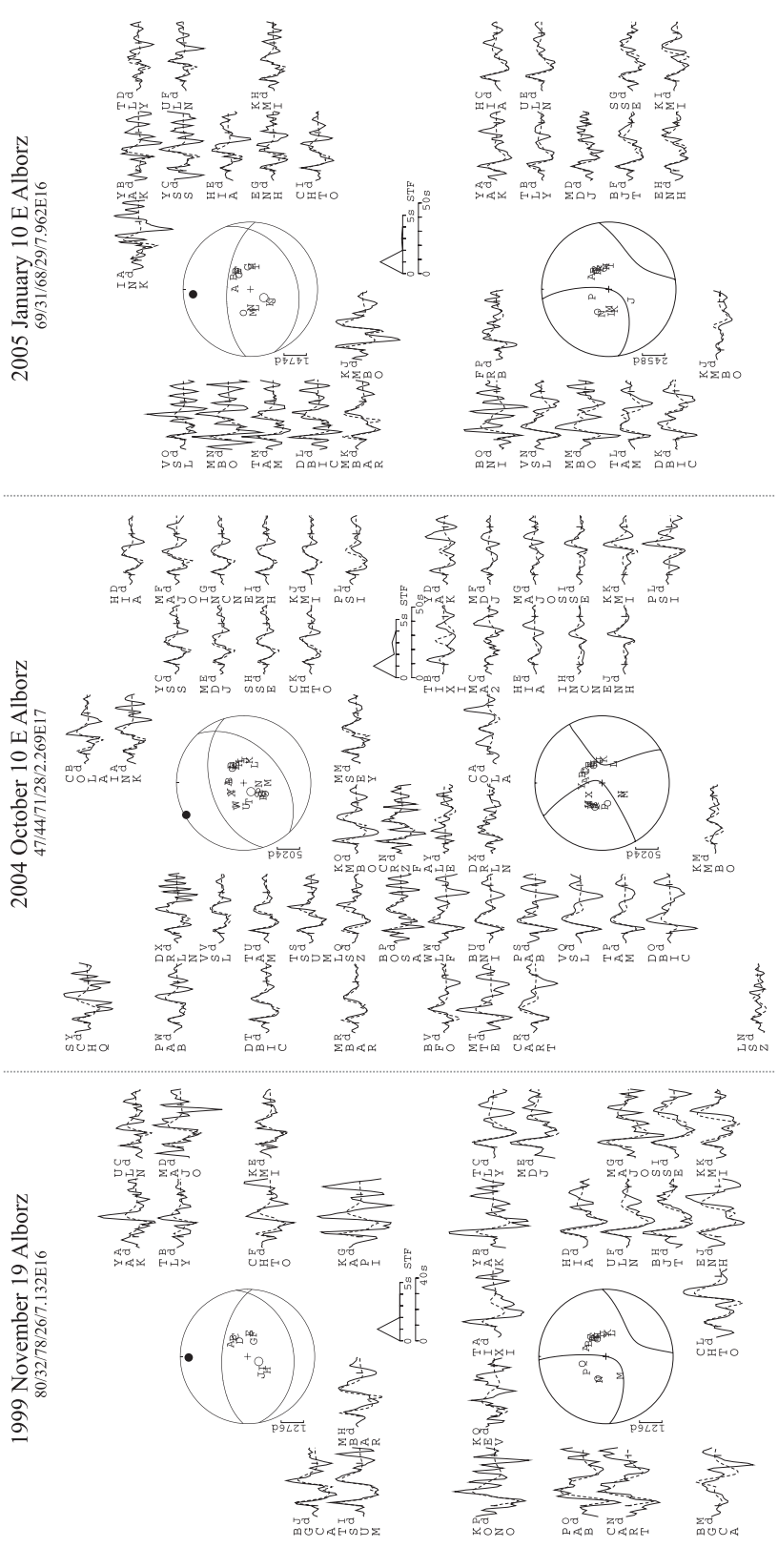

Figure 3. *P* and *SH* waveforms for the 1999, 2004 and 2005 earthquakes in the SCL of NE Iran. The event header shows the strike, dip, rake, centroid depth and scalar seismic moment (in Nm) of the best-fitting solution. The upper focal sphere shows a lower hemisphere stereographic projection of the *P* waveform nodal planes, along with positions of the seismic stations used in the inversion. The lower focal sphere shows the *SH* nodal planes. Capital letters next to the station codes indicate their position on the focal sphere, and are ordered clockwise by azimuth, starting at north. Solid lines show observed waveforms, and dashed lines show synthetics. The inversion window is marked by vertical lines on each waveform. The source time function (STF) is shown, along with time scale for the waveforms. The amplitude scales for the waveforms are shown below each focal sphere.

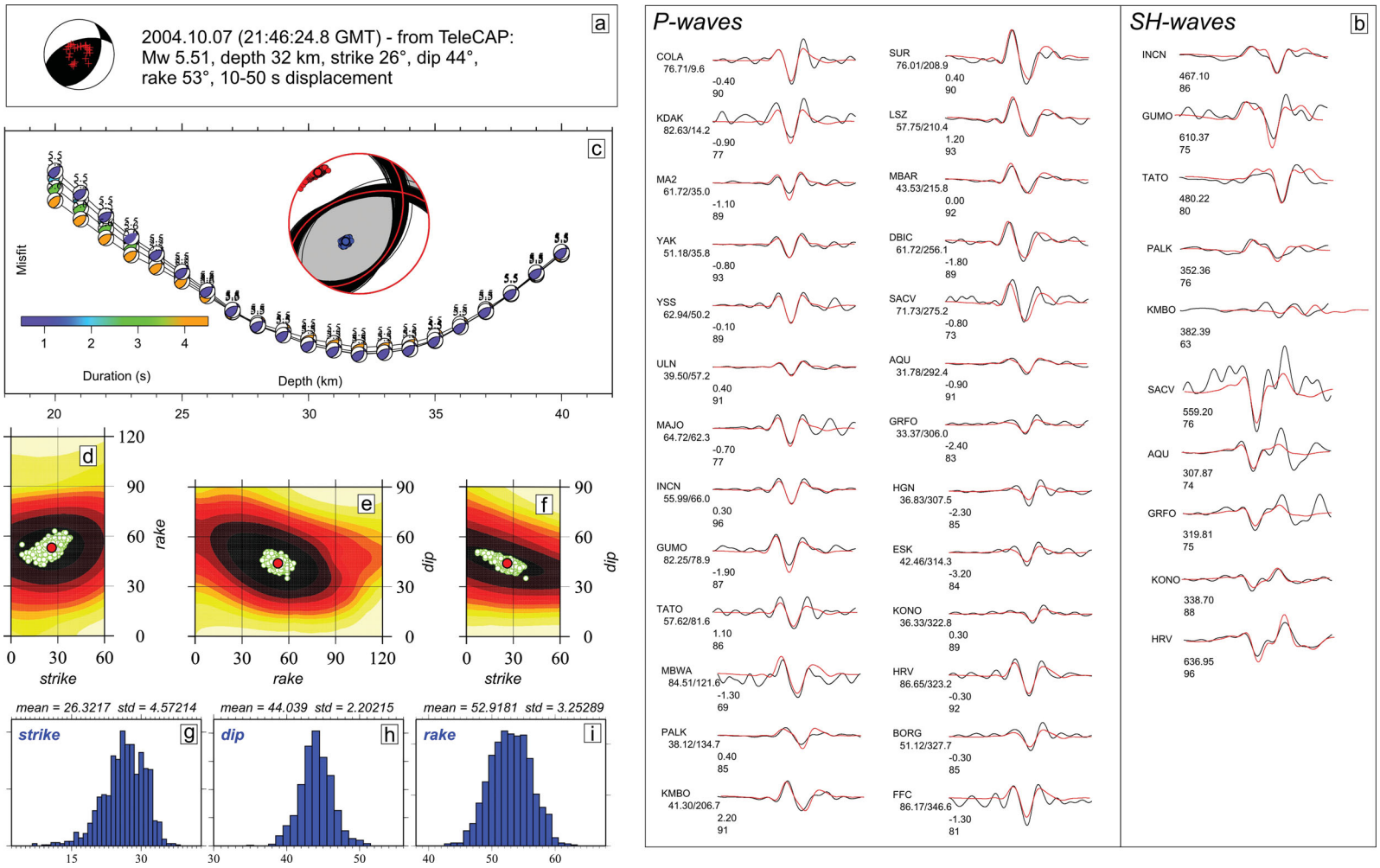

Figure 4. (a) Best-fitting fault plane solution for the 2004 October 7 earthquake determined using the Cut-and-Paste method. Red crosses show station distributions used in the inversion. (b) Teleseismic waveform fitting and the corresponding source parameters for the best-fitting solution. Black is the data and red is the synthetic. Both *P* and *SH* waveforms are used in the inversion. (c) Misfit function for a range of depths and durations for the 2004 event. Different durations cause very little difference in waveform misfit, and therefore have little trade-off with depth. All misfit curves for different durations show well-defined minimums at 31–33 km. The solution outlined in red shows the optimal focal mechanism. Solutions outlined in black show 1000 bootstrapping results. Red and blue dots show *P*- and *T*-axes for all 1000 focal mechanisms. (d, e, f) Optimal focal mechanism (red dots) and the 1000 bootstrapping focal mechanisms (small green dots) plotted over the misfit function. (g, h, i) Histograms of strike, dip and rake from the 1000 bootstrapping solutions. The titles show corresponding means and standard deviations for strike, dip and rake.

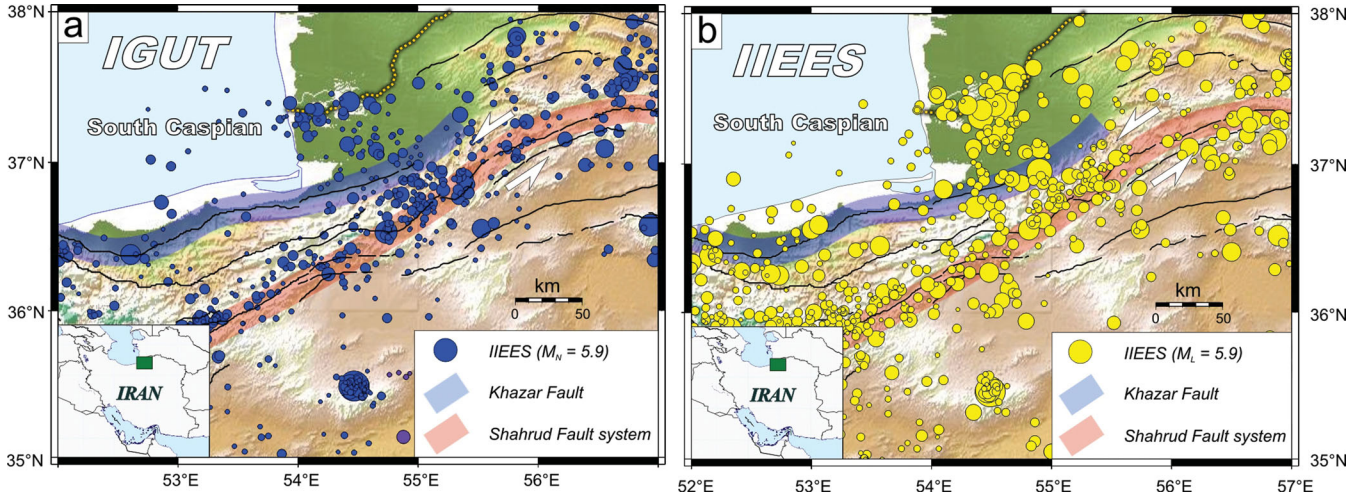

Figure 5. (a) Topographic map of showing seismicity (blue circles) of the SCL region recorded by the IGUT network between 2006 and 2010 (only events with rms $\leq$ 0.4 s are shown). (b) Seismicity of the SCL recorded by the IIEES network between 2004 and 2010. Only events recorded by a minimum of four stations and with magnitudes greater than 2.5 are shown (yellow circles).

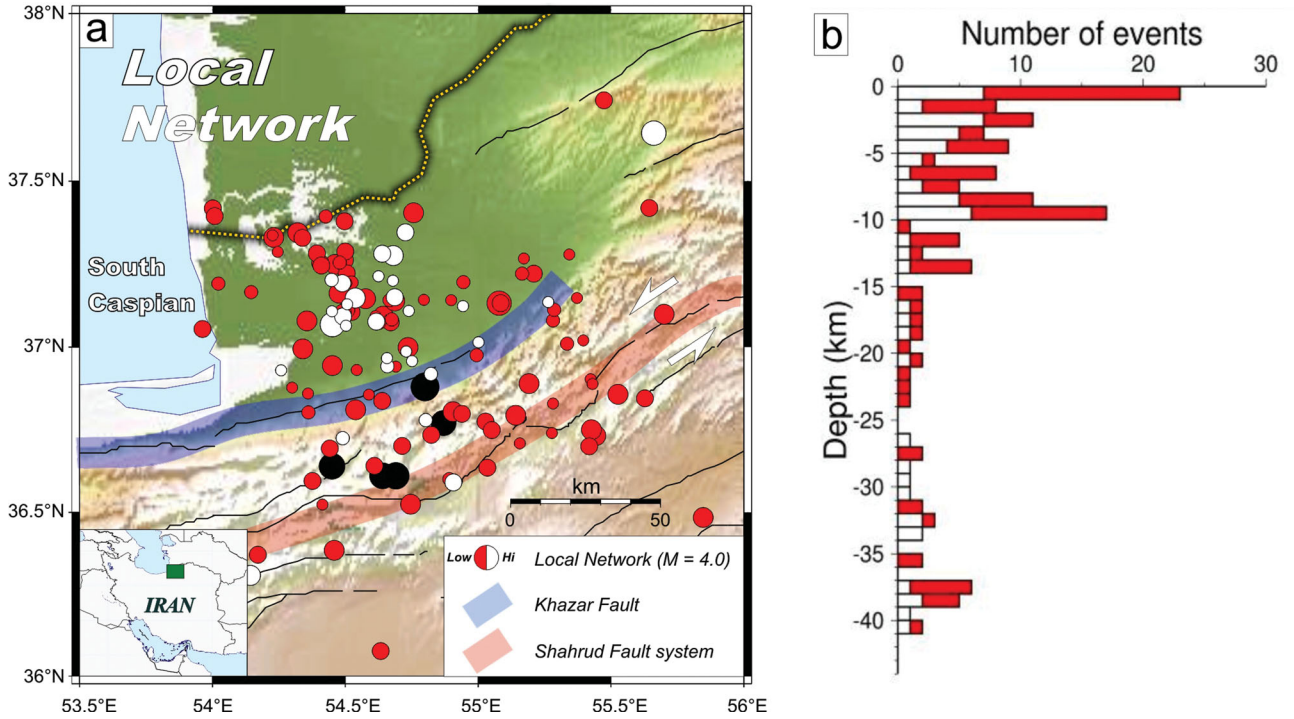

Figure 6. (a) Seismicity recorded by our local network. Higher quality event locations are shown by white circles (recorded by a minimum of four stations, maximum gap azimuth of 270°, horizontal and vertical errors $\leq$5 km and rms less than 0.5 s). Lower quality locations are shown in red. Black circles show aftershocks of the 1985 Gorgan earthquake located by USGS. (b) Depth distribution of events recorded by the local network. High and lower quality depths are shown in white and red, respectively. The majority of events occur in the upper 15 km, although micro-earthquakes occur all the way down to the Moho at 41 km.

both events are within error ($\pm$5 km) of the Moho (41 km), and therefore probably occur in the base of the crust. Mechanisms 5 and 8 may reflect left-lateral oblique shortening on the Khazar fault, with similar depths as aftershocks from the 2004 Baladeh earthquake in the Central Alborz (Tatar *et al.* 2007). The red solution in Fig. 7 shows the focal mechanism for the 1985 Gorgan earthquake (Priestley *et al.* 1994), which probably ruptured the south-dipping Khazar fault.

4.4 Results: velocity structure of the SCL

Table 4 shows our initial and final velocity models, calculated by inversion of traveltimes. At depths shallower than the Moho, the range of velocities is between 6 and 6.7 km s^{-1} (Nemati *et al.* 2010).

Because the majority of the events are located shallower than 20 km, we could not estimate the velocity for the deeper layers. We

Table 1. Source parameters of significant instrumentally recorded earthquakes occurring in NE Iran over the last 30 yr (Fig. 1). Except where constrained by body-waveform modelling, locations and depths for all events are taken from Engdahl *et al.* (2006, prior to 2005), and the updated catalogue of Engdahl *et al.* (1998, after 2005). Data sources are as follows: 1, Priestley *et al.* (1994); 2, this study; 3, Global CMT catalogue; 4, Tatar *et al.* (2007).

Eq. no.	Date	Time (GMT)	Latitude (°N)	Longitude (°E)	Approximate location	M_w (Nm^{-1})	Depth (km)	Strike (°)	Dip (°)	Rake (°)	Source
1	1970.07.30	00:52:20	37.84	55.89	Karnaveh	6.4	11	293	56	−150	1
2	1985.10.29	14:23:05	36.83	54.87	East Alborz	6.2	13	246	66	71	1
3	1999.11.19	04:40:25	37.30	54.39	South Caspian	5.4	26	80	32	78	2
4	1999.11.26	04:27:22	36.92	54.89	East Alborz	5.3	4	106	22	58	3
5	2000.08.16	12:53:01	36.73	54.38	East Alborz	4.9	15	240	34	78	3
6	2004.05.26	12:38:46	36.26	51.57	Central Alborz	6.3	22	110	34	76	4
7	2004.10.07	21:46:19	37.14	54.47	South Caspian	5.5	28	47	44	71	2
8	2005.01.10	18:47:30	37.06	54.53	South Caspian	5.2	29	69	31	68	2

Table 2. Nearest station distances, number of *P* and *S* readings and azimuthal gaps used to determine the depths for each micro-earthquake.

Date	HHMM	SS	Lat (°)	Lat (′)	Long (°)	Long (′)	Depth (km)	Mag.	Gap (°)	P+Sno	Dmin (km)	Rms (S)
90815	444	41.34	36	48.15	54	21.71	15.1	1.0	208	10	14.8	0.03
80827	615	13.85	35	34.23	53	12.2	16.0	2.0	127	12	27.4	0.2
91116	1940	37.05	37	5.53	54	29.47	16.1	2.0	76	40	15.8	0.5
91111	1948	27.48	37	4.8	55	16.95	17.0	1.0	250	10	8.7	0.31
100219	559	45.24	37	8.15	55	15.85	17.1	0.5	123	12	12.6	0.15
81013	1806	23.68	37	3.26	53	57.74	18.0	2.0	247	22	22.4	0.27
91209	1859	23.04	36	52.63	54	18.02	18.9	0.5	157	10	24.6	0.1
91203	1505	13.08	37	8.88	54	32.24	19.0	3.0	117	72	15	0.45
90920	1938	49.4	37	0.58	55	20.08	19.5	1.0	264	10	11.9	0.1
91111	208	1.74	36	56.55	54	39.48	20.2	1.0	232	10	21.9	0.03
70426	236	50.84	35	26.26	54	14.88	20.4	2.0	128	24	30.5	0.41
90815	844	7.94	37	8.5	54	39.99	21.7	1.0	204	10	7.3	0.12
100115	1739	25.44	36	35.71	54	22.6	22.8	2.0	261	14	15.8	0.15
90821	927	12.45	36	50.26	54	38.37	23.6	2.0	152	18	20.8	0.15
90920	907	10.44	37	7.46	54	56.57	26.2	0.5	173	10	25.3	0.1
60409	732	40.15	35	2.78	54	2.83	27.6	2.0	221	20	32.9	0.14
60424	1911	23.94	36	56.64	54	27.11	27.7	3.0	169	24	29	0.31
91114	1621	5.73	36	55.1	54	49.31	28.3	1.0	134	10	30.3	0.19
90817	1841	34.51	36	43.47	54	29.4	30.0	1.0	218	10	1.8	0.1
91017	1404	19.21	37	4.63	54	37.03	30.7	2.0	101	26	15.5	0.17
91101	3	40.15	37	4.99	54	40.47	31.1	1.0	83	24	13.5	0.42
91203	1546	30.79	37	4.4	54	37.69	32.0	1.0	177	10	15.5	0.1
100122	2026	27.18	37	6.54	54	44.36	32.1	0.5	106	26	11.4	0.39
100113	1744	51.54	37	3.89	54	30.14	32.8	0.5	106	12	22.8	0.25
90927	1929	41.8	36	56.46	54	41.45	32.9	0.5	191	14	22.2	0.23
100104	28	39.85	37	12.83	54	37.47	33.9	0.5	97	22	6	0.34
100103	2132	30.9	37	12.14	54	26.9	34.0	1.0	149	20	4.7	0.25
91015	2154	10.29	37	6.2	54	29.43	35.1	2.0	164	16	14.6	0.16
91223	329	5.7	37	5.61	54	36.83	36.0	0.5	167	12	14	0.13
100130	552	16.35	37	12.02	54	40.77	37.1	0.5	86	28	1.1	0.31
100106	1803	18.35	37	9.97	54	8.76	37.4	1.0	268	20	7.4	0.23
91012	2209	8.15	37	15.31	54	28.77	37.6	1.0	227	10	19.6	0.09
91015	2324	21.15	37	6.75	54	30.26	37.6	2.0	156	16	13.7	0.14
90718	2145	9.79	36	51.57	54	21.62	37.9	0.5	148	12	19.8	0.43
91218	1502	54.43	37	6.39	54	31.42	38.0	2.0	88	20	14.7	0.3
91117	2029	37.56	37	17.24	54	14.79	38.2	0.5	264	20	21.7	0.47
90917	511	8.92	37	16.75	55	20.58	38.4	0.5	214	10	11.6	0.03
100112	1506	50.47	37	11.7	54	31.42	38.4	1.0	136	14	5.7	0.28
91229	105	23.19	37	11.54	54	29.34	38.8	2.0	96	18	4.7	0.23
91020	2146	25.42	37	6.47	54	26.98	38.9	0.5	189	14	14.3	0.11
91026	1722	0.36	37	16.89	54	38.34	39.2	2.0	131	22	9.7	0.19
91106	519	20.62	37	16.57	54	40.86	40.1	3.0	114	26	8	0.34
90902	1615	28.1	37	8.56	54	47.79	41.0	0.5	123	10	30.4	0.02

therefore used traveltimes of refracted waves from distant events to estimate the depth and velocity structure deeper than 20 km. Using 846 traveltimes recorded in the IGUT network, we computed a *P*-wave velocity of 8.2 km s^{-1} for the upper mantle with a Moho depth of 41 km. This velocity is consistent with the 8.2–8.5 km s^{-1} velocity estimated from Pn tomography for this region (personal communication, Abdoreza Ghods, 2012). The computed average velocity (~6.5 km s^{-1}) of the upper crust, shown by the slope of the

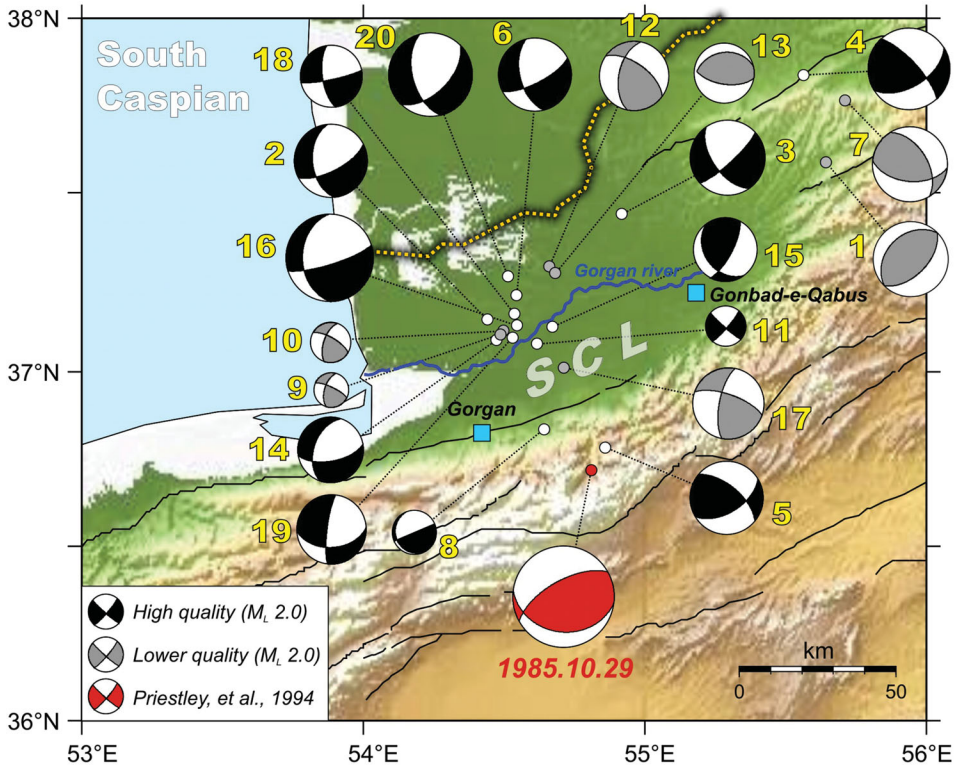

Figure 7. Topographic map showing fault plane solutions for 20 micro-earthquakes recorded by our local network. Each event was recorded by at least five stations, with an azimuthal gap less than 180° and horizontal and depth uncertainties less than 5 km (see Table 3 for details). Black solutions are higher quality, grey solutions are lower quality. Red solution is for the 1985 October 29 Gorgan earthquake (Priestley *et al.* 1994).

Table 3. Source parameters of 20 micro-earthquakes for which we were able to generate reliable first-motion focal mechanisms (Fig. 7)—see also Fig. A1. "∗" Denotes lower quality focal mechanisms.

Number	Year	Month	Day	Hr/Min	Sec.	Long. (°E)	Lat. (°N)	Depth (km)	Strike (°)	Dip (°)	Rake (°)	Mag. (M_L)
1*	2006	11	11	1703	44.8	55.644	37.593	7.5	45.0	55.0	90.0	4.1
2	2007	8	30	1649	29.2	54.440	37.148	13.0	62.9	67.5	−45.9	4.0
3	2008	5	15	522	6.5	54.917	37.446	10.8	47.3	78.7	−33.3	4.1
4	2008	8	1	754	44.8	55.564	37.840	2.9	58.7	54.4	19.5	4.5
5	2008	8	25	337	44.8	54.860	36.784	23.1	58.7	57.2	32.7	4.0
6	2009	2	20	1948	25.3	54.545	37.216	7.4	63.0	71.3	−36.0	4.0
7*	2009	4	15	337	44.8	55.710	37.771	9.4	95.4	52.2	50.8	4.1
8	2009	8	21	927	12.5	54.642	36.836	23.5	246.7	90.0	75.0	2.4
9*	2009	10	15	2154	10.3	54.486	37.106	35.1	295.2	76.0	32.4	1.9
10*	2009	10	15	2324	21.1	54.499	37.116	38.3	300.0	70.0	30.0	2.2
11	2009	10	17	1404	19.2	54.616	37.078	31.3	40.7	81.8	−5.8	2.2
12*	2009	10	26	1721	12.0	54.661	37.300	44.3	305.5	60.5	42.4	3.8
13*	2009	11	6	519	20.6	54.682	37.278	40.9	257.1	31.5	70.6	3.3
14	2009	11	16	1940	37.0	54.473	37.091	15.0	79.9	62.0	−49.5	3.6
15	2009	11	16	2346	20.0	54.670	37.126	0.0	143.5	35.5	30.6	3.5
16	2009	12	3	1505	13.0	54.547	37.130	15.0	72.8	77.8	−54.1	4.8
17*	2009	12	3	2033	0.2	54.711	37.012	15.0	289.1	69.3	22.2	3.9
18	2009	12	14	1905	23.8	54.537	37.164	19.3	78.3	81.7	−23.7	3.4
19	2009	12	18	1446	39.5	54.530	37.097	17.3	86.9	46.9	−14.5	3.8
20	2010	3	4	324	22.8	54.514	37.272	23.1	45.1	54.6	−45.3	4.6

lower left fitted line in Fig. 8, is consistent with the result of the 1-D inversion. This is not a unique method of Moho determination; the refraction range in Fig. 8 indicates ∼3 km uncertainty in the Moho depth. Furthermore, the refracted traveltimes of distant events is sensitive only to horizontal discontinuities. Nevertheless, despite location uncertainties of ∼5 km, and possible artifacts due to lateral heterogeneities for the regionally recorded events this method is efficient for resolving shallow discontinuities (<45 km).

5 DISCUSSION

5.1 Summary of results

In this study we use both teleseismic and local network seismicity data to investigate the subsurface tectonics of the SCL region of NE Iran. Data from our local seismic network is used to compute the ratio of V_P/V_S (about 1.70), while inversion of local travel-times from reliable events yields a velocity range in the crust of

Table 4. Starting velocity structure (Mangino & Priestley 1998), and final velocity structure computed using locally recorded events.

Initial velocity model (Mangino & Priestley 1998)		Final velocity model	
Velocity (km s^{-1})	Depth (km)	Velocity (km s^{-1})	Depth (km)
5.5	0	6.0	0
6.3	7	6.2	6
8.0	33	6.4	12
		6.7	20
		8.2	41

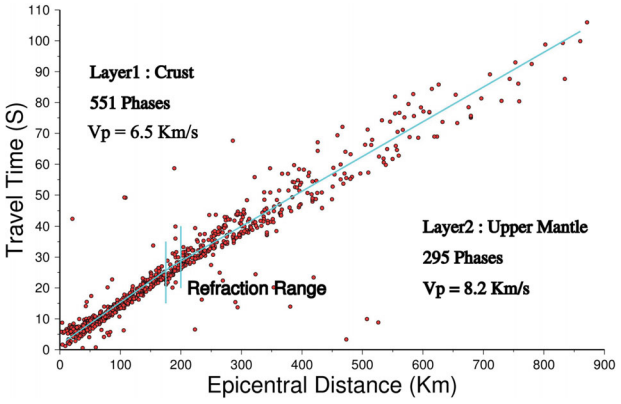

Figure 8. Estimation of Moho depth and upper mantle velocity using traveltimes from 846 distant earthquakes. Only earthquakes with RMS residuals ≤0.5 s, horizontal and vertical errors less than 10 km, and a maximum azimuthal gap up to 180° were used in the analysis. We estimate 8.2 km s^{-1} for the velocity of the upper mantle, given by the slope of the best-fitting line of Pn.

6.0–6.7 km s^{-1}, consistent with other studies in the area (Mangino & Priestley 1998). Using traveltimes of refracted waves from distant events, we obtain a velocity of 8.2 km s^{-1} for the upper mantle Pn wave velocity and a Moho depth of 41 km.

For the Tehran region of the Central Alborz, Ashtari *et al.* (2005) computed a Moho depth of 34 km and 8.0 km s^{-1} for the *P*-wave velocity in the upper mantle using locally recorded micro-earthquakes. Sodoudi *et al.* (2009) found deeper Moho depths beneath the Central Alborz (51–54 km), using *P*- and *S*-receiver function methods. However, a more recent study by Radjaee *et al.* (2010), which uses simultaneous joint inversion of teleseismic receiver functions with fundamental mode Rayleigh wave group velocity measurements across the entire Central Alborz, gives even deeper Moho depths of 55–58 km beneath the range, 48 ± 2.5 km immediately south of the Alborz (i.e. Central Iran), and 46 ± 2.5 km immediately north of the Alborz (i.e. SCL). Using a partitioned waveform inversion method, Shad Manaman *et al.* (2011) image the *S*-velocity structure of the Iranian Plateau, and find similar Moho values as Radjaee *et al.* (2010) for the Central Alborz of 55–60 km, although they obtain significantly lower values of 35–37 km for the West and East Alborz regions. One explanation for the different estimates of Sodoudi *et al.* (2009) and Radjaee *et al.* (2010) is that Sodoudi *et al.* (2009) use the IASPIE91 earth model (Kennett & Enghdal 1991) to convert the Moho *Ps* delay times to an interface conversion depth. The IASPIE91 model is faster (average V_s 3.81 km s^{-1}) than the average velocity Radjaee *et al.* (2010) find for the central Alborz region (V_s 3.59 km s^{-1}) resulting in a 3–4 km deeper depth estimate. Based on the results of Radjaee *et al.* (2010) and Shad Manaman *et al.* (2011), the Alborz appear to have a moderate crustal root but of insufficient thickness to compensate the elevation of the range, where numerous peaks rise above 3000 m. The analysis of free-air gravity shows that the elevation of the Alborz Mountains is largely supported by the elastic strength of the Iranian Plate, the South Caspian Plate or both (Radjaee *et al.* 2010). Our Moho depth estimate of 41 km for the SCL region north of Gorgan is therefore broadly consistent with the 46 km estimate of Radjaee *et al.* (2010) for the SCL north of the Central Alborz range. However, it raises questions regarding the depth of the Moho beneath the East Alborz mountains south of Gorgan, where Nemati *et al.* (2011) computed a *P*-wave velocity for the upper mantle of 8.0 km s^{-1} and a Moho depth of 34 km using 458 traveltimes recorded in the IGUT network, and Shad Manaman *et al.* (2011) obtain a Moho depth between 35 and 37 km.

The crustal velocity model and depth distribution of micro-earthquakes suggests a sedimentary cover of ∼6 km, similar to the 7 km depth in the NE Alborz region, calculated using receiver functions analysis (Mangino & Priestley 1998). Our estimates are less consistent with the 10 km estimate of Tatar *et al.* (2007) for the north-central Alborz, which ruptured in the 2004 Baladeh earthquake. Although the majority of micro-earthquakes occur in the upper 15 km of the crust, events occur all the way down to the Moho at 41 km depth, suggesting the South Caspian crust is strong throughout.

Earthquake epicentres recorded between 2004 and 2010 by the IGUT and IIEES regional networks are focused on the left-lateral Shahrud fault system, within the southern half of the East Alborz mountains south of our study area. Activity on the Khazar fault is relatively low, although a large earthquake probably ruptured this section of the fault in 1985. Three mid-sized earthquakes, with relatively deep depths for Iran (∼30 km), occurred north of the Khazar fault within the stable SCL in 1999, 2004 and 2005. A small cluster of micro-earthquakes recorded between 2009 and 2010 also coincide with these deep earthquakes. These events occur mostly at shallow depths, and focal mechanisms for the largest events indicate predominantly strike-slip motion (probably left-lateral on NE–SW-oriented planes), with a small normal component in the shallower events.

5.2 Variation of deformation-style with depth in the SCL

A cross-section through the SCL crust is shown in Fig. 9, which helps illustrate the subsurface deformation occurring at the present day. Earthquakes larger than M_w 5.2 are shown in blue (Global CMT) and red (Priestley *et al.* 1994). Grey and black solutions are micro-earthquakes (M_L 1.9–4.8) recorded by our local network. Earthquakes south of the Alborz range front project from depths of <25 km to the Khazar fault, which strikes along the edge of the range front, and is poorly expressed in the geomorphology in this region. Seismicity within the SCL north of the range front is broadly grouped into deep thrust earthquakes (30–41 km), and shallow left-lateral micro-earthquakes with a small normal component (<20 km). These shallow events lie along-strike from known left-lateral strike-slip faults to the NE (e.g. at Karnaveh, Fig. 10, and Kara Kala, Fig. 11). Therefore, they may represent re-activation of similar structures which have been buried by sediments within the SCB. Alternatively, they could simply be shallow earthquakes responding to stress changes after the earlier 1999, 2004 and 2005 events. Moho depth estimates in this region (Mangino & Priestley 1998, and this study) increase from 35 to 41 km between distances of ∼100 km and ∼50 km north of the Alborz range front (Fig. 9c). Consequently, the 1999, 2004 and 2005 events all occur near the base of the crust, implying the South Caspian crust is strong throughout (see also Jackson 2002). Therefore, the pattern of deep thrust and

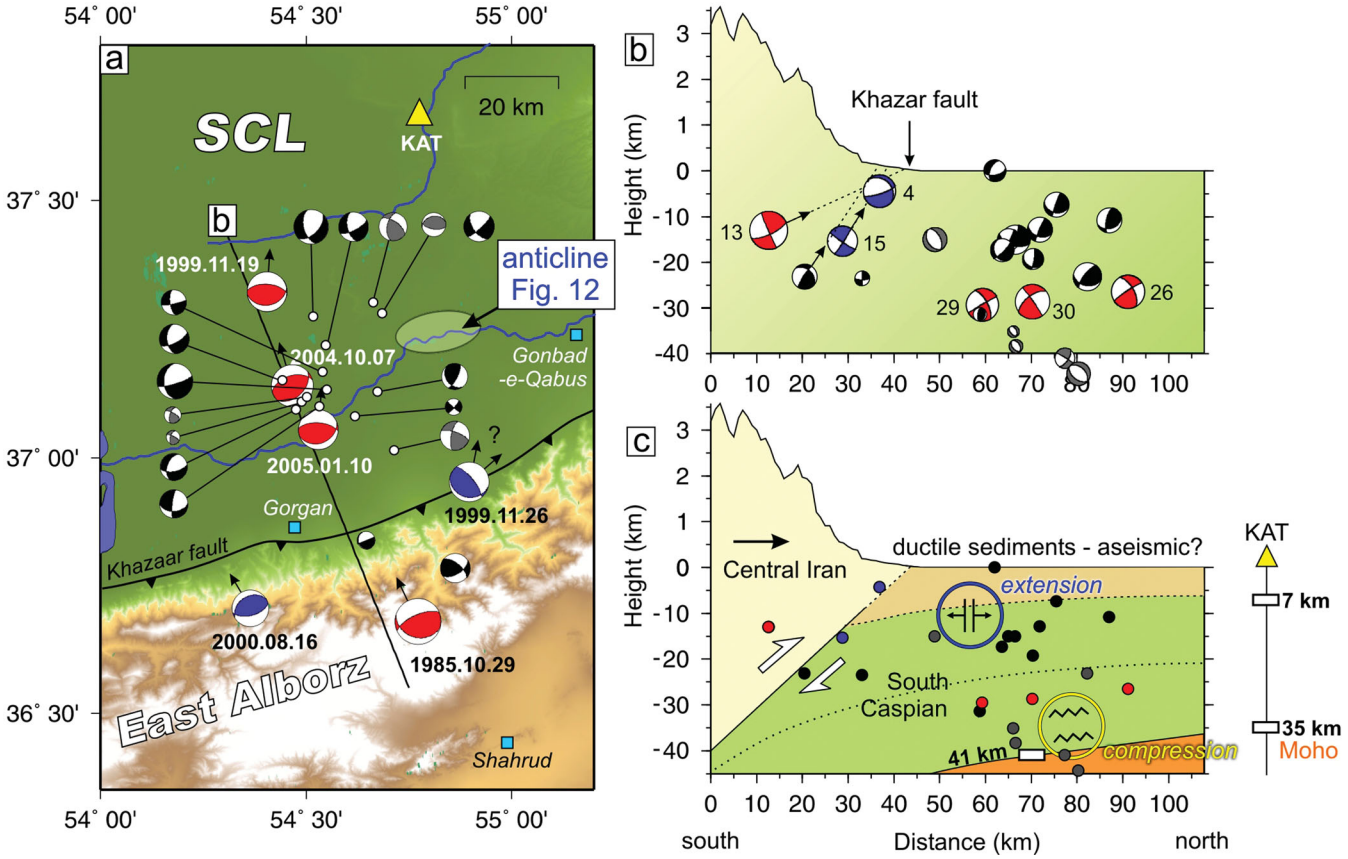

Figure 9. (a) Recent seismicity along the eastern end of the Khazar thrust fault. The fault runs along the foot of the Alborz mountains (black line) and is probably blind. Blue lines show major rivers. The red solution is for the 1985 Gorgan earthquake (M_w 6.2), which probably occurred on the Khazar thrust (from the body-waveform solution of Priestley *et al.* 1994). Blue solutions are from the Global CMT catalogue, and show other large earthquakes in the area. Black arrows show likely slip vectors for the earthquakes, assuming slip on the S-dipping Khazar fault, and a gently N-dipping plane in the base of the South Caspian crust (see also c). Black and grey solutions are for micro-earthquakes recorded by our local network. The yellow triangle (KAT) shows the location of receiver function estimates of the crustal structure (Mangino & Priestley 1998; Raven 2005). (b) Cross-section through the crust and fault plane solutions, along the black line in (a), showing the depth distribution of earthquakes. (c) Tectonic interpretation of the crustal section in (b). Black arrow shows the direction of motion between of Central Iran, relative to the South Caspian. The Moho depth increases southward from 35 km (near KAT) to 41 km (beneath our local network). the depth of the sedimentary cover is 6–7 km (this study, and Mangino & Priestley 1998; Raven 2005). Compression occurs in the base of the crust, and extension occurs near the surface, as the South Caspian is bent beneath the Alborz mountains.

shallow normal earthquakes may result from bending of the South Caspian crust beneath the over-riding Alborz mountains and Central Iran. Thus, the Alborz mountains are supported, at least in part, by the strong South Caspian crust (e.g Radjaee *et al.* 2010). The separation by depth of shallow normal and deep thrust events associated with bending is common in the oceans, and seen on the outer rises of many subduction zones (e.g. Chapple & Forsyth 1979). However, it much less common in the continents, with the clearest examples coming from Central Asia, where northern India (Jackson 2002) and the Tarim basin (Sloan *et al.* 2011) underthrust Tibet. Nevertheless, the transtensional rather than normal mechanisms of the shallow micro-earthquakes recorded by our local network could result simply from the westward motion of the South Caspian block relative to Central Iran and Eurasia, rather than a response to bending of the rigid South Caspian crust beneath the Alborz (Javidfakhr *et al.* 2011). Furthermore, despite deep thrust events having occurred in this region, there have been no recorded large normal earthquakes, as might be expected with such a bending mechanism. Therefore, it is also possible the 1999, 2004 and 2005 events are related to thrust faults stepping northward of the Alborz range front. Similar basinward migration of thrust faults is seen elsewhere in the East Alborz and Sabzevar mountains (Hollingsworth *et al.* 2010a), elsewhere in Iran (Berberian *et al.* 2001; Walker 2003), and is typical of older continental thrust systems such as the Alps and Himalayas (Boyer & Elliott 1982).

5.3 Tectonic geomorphology: observations of the West Kopeh Dagh region

Although micro-earthquakes may not always provide a clear picture of the regional tectonics, due to their relatively small contribution to the regional seismic moment release, compared with larger earthquakes (e.g. $M_w > 5.2$), these events lie along strike from NE–SW left-lateral fault systems to the east, near Karnaveh and Kara Kala, which are known to be seismogenic. On the 1970 July 30, the Karnaveh earthquake (M_w 6.4) occurred ~100 km NE of the area covered by our local network, where the Western Kopeh Dagh mountains drop down to the meet the SCL (Fig. 1). The earthquake caused widespread destruction to villages in the region, killing ~200 people (Ambraseys *et al.* 1971). No clear surface rupture was reported, although the rupture may not have propagated through the extensive loess deposits covering the area, or may have degraded rapidly after

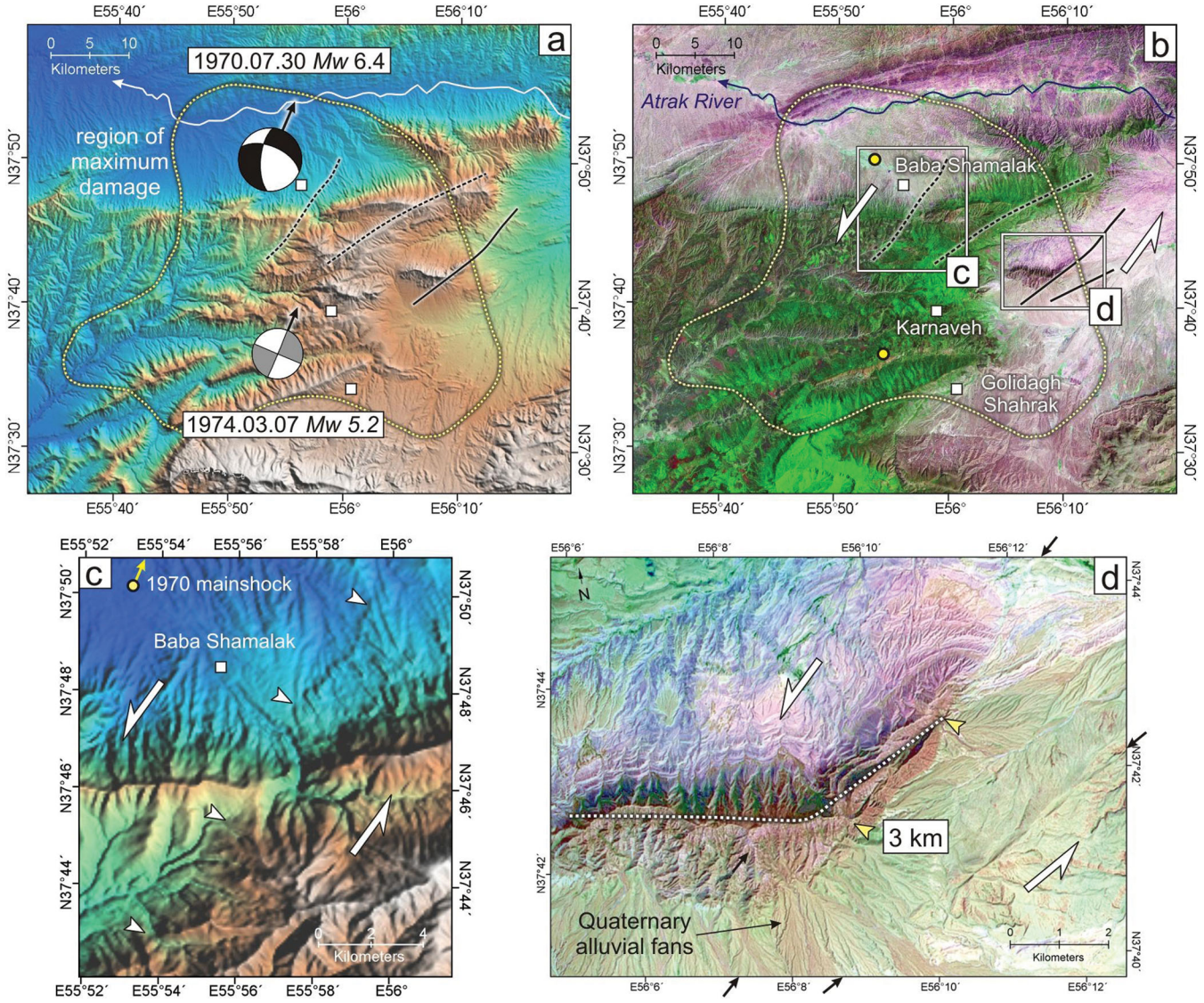

Figure 10. (a) Topographic map of the Karnaveh region, which lies on the northern flanks of the Alborz mountains. Yellow dotted line shows the region of maximum structural damage resulting from the 1970 July 30 Karnaveh earthquake (Ambraseys *et al.* 1971). Black lines show faults identified in the geomorphology and geology. The fault plane solution for this earthquake, from body-waveform modelling, is shown in black (Priestley *et al.* 1994). A smaller event in 1974 March 7, also occurred within this epicentral region of the 1970 earthquake (grey solution, Jackson & Fitch 1979). Black arrows show the slip vectors of both earthquakes (south relative to north). (b) Landsat7 satellite image of the Karnaveh region. Vegetation (green areas), covers loess deposits throughout the epicentral region. (c) Topographic map of the 1970 main shock region. A step in the topography (up to the east) occurs along a NE–SW trend, cutting across river deposits 2 km east of Baba Shamalak (marked by white pointers). Yellow arrow shows the slip vector of the Karnaveh earthquake. (d) Landsat7 satellite image of the eastern epicentral region, which is not covered by vegetation. Two NE–SW-striking faults displace Mesozoic rocks and Quaternary alluvial deposits between the black arrows. Apparent drag of the geology into the fault zone of the western fault (white dotted line shows the fold crest) indicates a minimum of 3 km left-lateral motion, highlighted by yellow pointers.

the earthquake (Fig. 10, see also Fig. 1 for location). The worst affected villages of Baba Shamalak (25 per cent of population killed), Karnaveh (<10 per cent) and Golidagh Shahrak (<10 per cent) span a distance of 30 km. Four subparallel NE–SW faults lie within this region of maximum destuction (Figs 10a and b), although only the eastern fault is clearly visible in satellite imagery; the other two are obscured by vegetation, and are inferred from lineations visible in the topography (Fig. 10c). One of these faults runs SW of Baba Shamalak, which lies 10 km east of the teleseismic epicentral location of Engdahl *et al.* (2006), and is visible as a small ridge uplifting Quaternary river deposits to the east (Fig. 10c). The orientation and sense of uplift is consistent with the left-lateral nodal plane in the solution of Priestley *et al.* (1994, see Fig. 10a), which also has a small normal component (down to the west) and Jackson & Fitch (1979), who recorded aftershocks aligned in a NE–SW direction. The two eastern faults, shown in Fig. 10(d), have similar lengths to the fault west of Baba Shamalak. Drag of the bedrock geology into the fault zone is consistent with left-lateral motion (3 km minimum offset estimated from deflection of a fold axis, white dotted line in Fig. 10d).

Another system of active left-lateral faults lies 50 km north of Karnaveh, near the town of Kara Kala in Turkmenistan (Fig. 11). Although the rocks offset Mesozoic geology, small river systems have been deflected across the fault against their drainage direction, suggesting they are active at the present-day. Active left-lateral shear on NE-SW striking faults both at Karnaveh and Kara Kala may partly

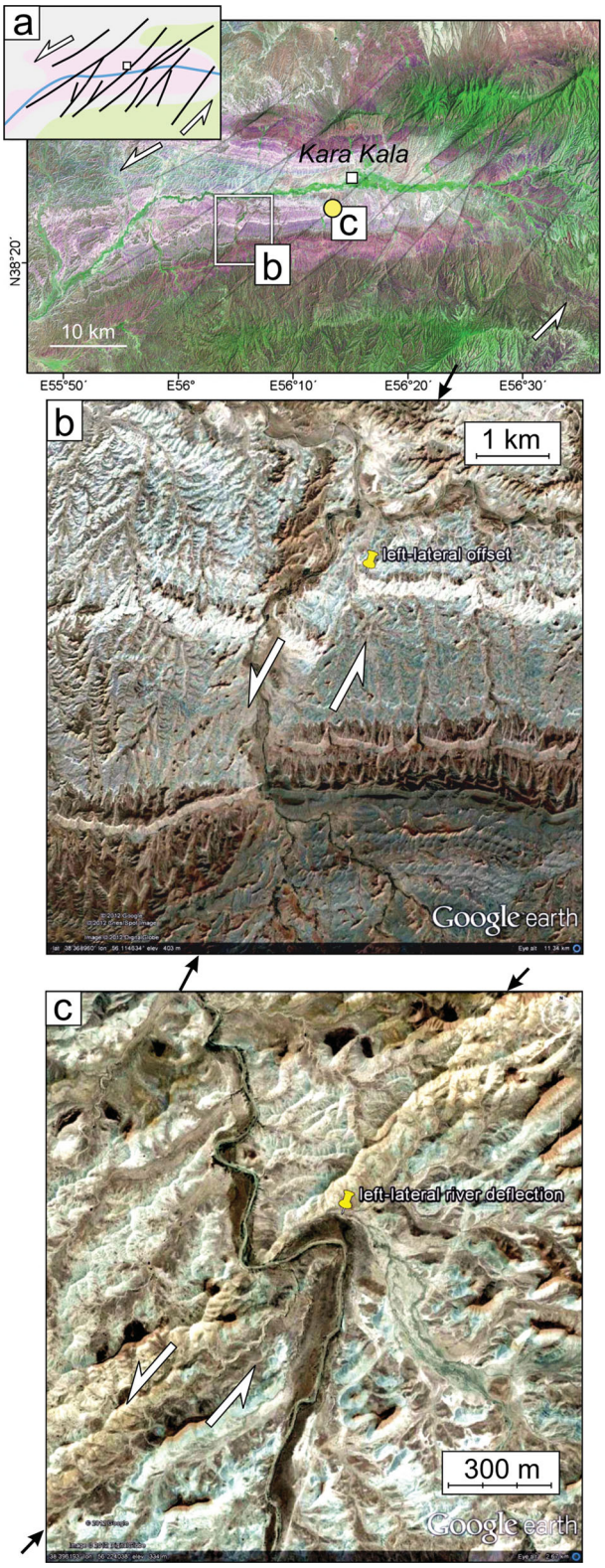

Figure 11. (a) Landsat7 satellite image of the western Kopeh Dagh mountains near the town of Kara Kala (Turkmenistan, see Fig. 5d for location). Pale grey lines show various left-lateral faults (see inset map for clearer image of active faults in this area). (b) SPOT satellite image (GoogleEarth) showing left-lateral displacement of Mesozoic geology across one of the left-lateral faults located 20 km SW of Kara Kala. (c) Quickbird satellite image showing left-lateral deflection of a river, and its associated terrace deposits, 5 km SW of Kara Kala.

accommodate the westward motion of the South Caspian/Western Kopeh Dagh regions (relative to Eurasia and Central Iran), in a similar manner to the Shahrud fault system to the south (Hollingsworth *et al.* 2008).

5.4 Tectonic geomorphology: expression of flexural bending in the SCL

A small topographic high occurs in the SCL, at the eastern end of the zone of micro-earthquakes recorded by our local network (Fig. 9). At this location (N37.25° E57.75°, see Fig. 12), a number of streams (dark green lines) appear to drain south into the west-draining Gorgan river (heavy blue line). A topographic profile across this area indicates the south draining streams (green lines) actually lie on a north-facing slope. Some of these streams have even reversed their flow direction (red lines), joining up with another west draining river to the north. Thus, a subtle topographic high appears to have formed in the late Quaternary, disrupting the drainage in this relatively flat area. One possibility is that, over time, buried left-lateral faults slipping with a small normal component have produced a small amount of footwall uplift, consistent with the focal mechanisms of micro-earthquakes in this region. If the faults could not propagate all the way to the surface, through the weak sedimentary cover, footwall uplift may have warped the overlying sediments to form a topographic high. Any diffuse extension occurring in the crest of the uplifted area may have been excavated by the Gorgan river. Repeated slip at depth would result in uplift of the area, and incision of the Gorgan river to maintain its current course. With continuing uplift, streams draining southward into the Gorgan river will have been back-tilted and abandoned. Figs 12(c) and (d) show two cartoons illustrating this concept. Although this hypothesis could potentially explain the formation of this bulge in the geomorphology, its lies only 25 km north of the range front, which may be too close to be caused by bending. In the neighbouring Kopeh Dagh mountain range, several hundred kilometres to the northeast, bending of the Turkmen foreland extends up 100 km north of the range (Maggi *et al.* 2000). The Kopeh Dagh foreland is unlikely to be significantly different from the East Alborz. An alternative explanation is that the normal component in the various micro-earthquakes could result from the overall westward motion of the SCB relative to NE Iran (Jackson *et al.* 2002; Javidfakhr *et al.* 2011), although this would not necessarily explain the depth separation of normal and thrust mechanisms. Uplift could also result from slip on a north-dipping thrust fault, although the decreasing elevation to the north of this area, and the proximity to the major south-sipping Khazar fault make this explanation unlikely.

6 CONCLUSIONS

Using a combination of data on the local and regional seismicity, crustal structure and tectonic geomorphology of the SCL region of NE Iran, we provide a relatively coherent picture of the active tectonics of this little-studied region. Inversion of earthquake traveltimes yields a velocity structure for the SCL crust, and a Moho depth of 41 km. Micro-earthquakes occur down to 41 km, while three thrust earthquakes in 1999, 2004 and 2005 occurred at depths of ∼30 km, implying shortening near the base of the South Caspian crust. Oblique-slip (left-lateral and normal) micro-earthquakes occur in the shallow crust (<20 km) above the deeper thrust events. If micro-earthquakes in this area are representative of the

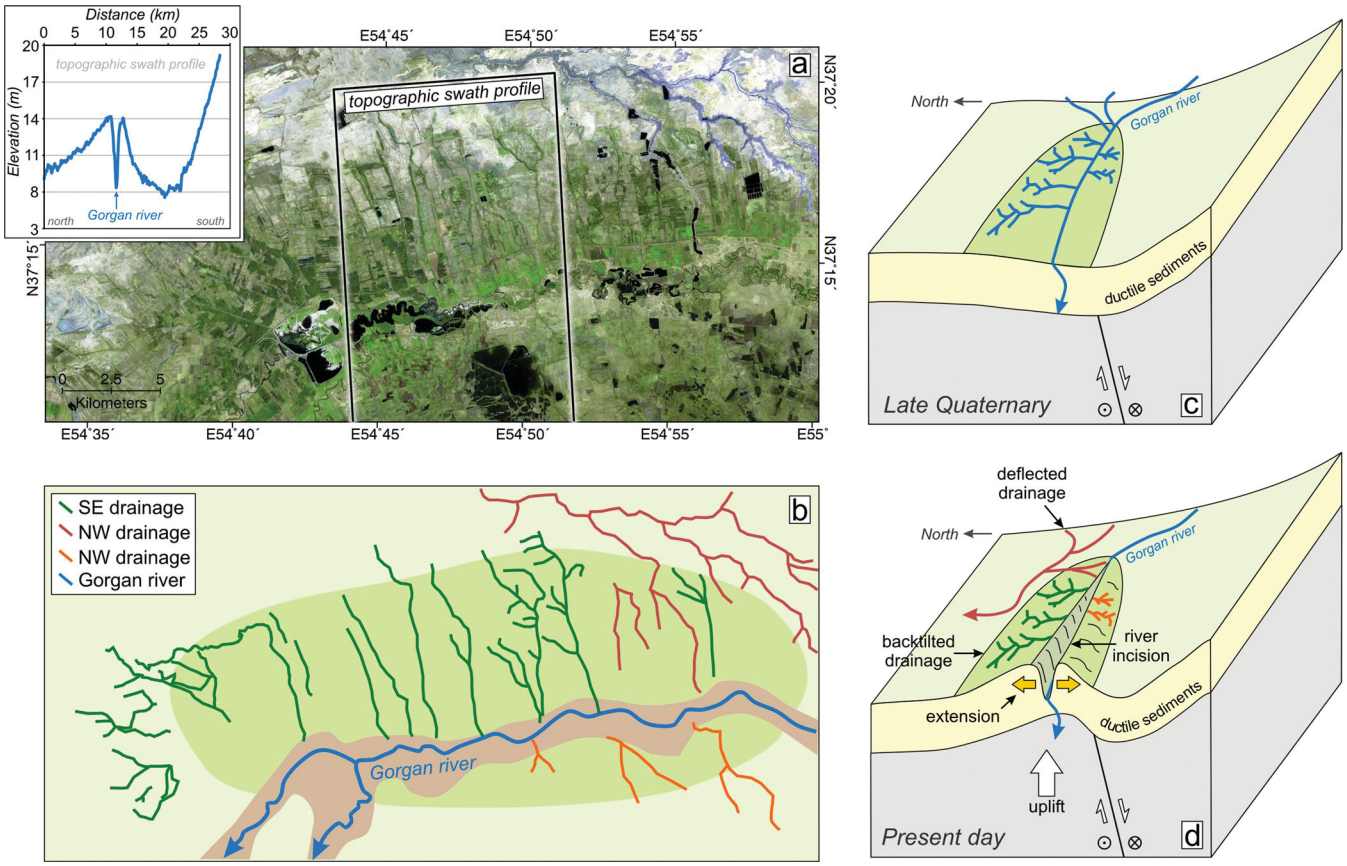

Figure 12. (a) Landsat7 satellite image of a topographic high which lies in the SCL northeast of Gorgan and west of Gonbad-e-Qabus (see Fig. 9 for location). Inset shows a 10-km-wide swath topographic profile across this anticline (black box in a). The Gorgan river flows along the axis of the anticline, through which it has incised. (b) Simplified interpretation of the geomorphology in (a). The dark green region corresponds to the regional of uplift. Dark green lines show streams which originally drained south into the Gorgan river (blue line). These rivers currently lie on a north-dipping slope (see inset figure in a), having been back-tilted and abandoned during the Holocene. Red lines show streams and rivers which originally drained south into the Gorgan river, which have now been deflected to the north, around the ridge. Orange lines show streams which drained north into the Gorgan river, which have been recently tilted south and abandoned. (c and d) Two cartoons showing how the drainage in (a) has evolved with time due to footwall uplift on shallow faults which slip with a small normal component of motion. Because of the extensive and ductile sediments which characterize the SCL, the faults do not propagate to the surface. However, continued uplift causes warping of the surface and uplift of an anticlinal ridge.

deformation produced by larger earthquakes, left-lateral shear, related to the westward extrusion of the SCB, may be accommodated within the SCL, north of the Alborz and Khazar fault. The pattern of shallow transtention and deep shortening may also be produced as the rigid/elastic South Caspian crust is thrust beneath the Alborz mountains, which it partially supports. Transtentional events may result from re-activation of pre-existing buried left-lateral faults, common in the region. Significant sedimentation and dense vegetation within the SCL obscures much of the fault-related geomorphology. Nevertheless, a small component of footwall uplift possibly associated with shallow events (assuming it is persistent over thousands of years), may be at least partially preserved in drainage systems throughout the area.

ACKNOWLEDGEMENTS

We thank the Geological Survey of Iran for organizing all aspects of the fieldwork, and providing seismological instruments. We also thank the IGUT and the IIEES in Iran, who kindly provided the records from their seismological networks. We are particularly grateful to the people and governor of Golestan province, who supported our study and wished to learn more about the seismic hazard posed by active faults in this region. We are grateful to James Jackson and an anonymous reviewer for their careful reviews. This study benefited from useful discussions on the geology and seismology of the region with Hamid Nazari, Mohammad Tatar and Shahryar Soleimani Azad. Ali Moradi provided important technical guidance. JH would like to thank the Gordon and Betty Moore Foundation and the Tectonic Observatory at Caltech for financial assistance. Various images in this paper were created using the public domain Generic Mapping Tools (GMT) software (Wessel & Smith 1998). Quickbird satellite images were obtained from GoogleEarth, Landsat7 images from the Global Land Cover Facility at the University of Maryland, and SRTM digital topography from the CGIAR Consortium for Spatial Information. This is Tectonic Observatory contribution number 224.

REFERENCES

Alavi, M., 1996. Tectonostratigraphic synthesis and structural style of the Alborz mountain system in northern Iran, *J. Geodyn.,* **21**(1), 1–33.

Allen, M., Jones, S., Ismail-Zadeh, A., Simmons, M. & Anderson, L., 2002. Onset of subduction as the cause of rapid Pliocene-Quaternary subsidence in the South Caspian Basin, *Geology,* **30,** 775–778.

Allen, M., Walker, R., Jackson, J., Blanc, E.-P., Talebian, M. & Ghassemi, M., 2006. Contrasting styles of convergence in the Arabia-Eurasia

collision: why escape tectonics does not occur in Iran, in *Postcollisional Tectonics and Magmatism in the Mediterranean Region and Asia,* pp. 579–589, eds Dilek, Y. & Pavlides, S., Vol. GSA Special Paper 409, Boulder, Colarado.

Allen, M., Kheirkhah, M., Emami, M. & Jones, S., 2011. Right-lateral shear across Iran and kinematic change in the Arabia-Eurasia collision zone, *Geophys. J. Int.,* **184,** 555–574.

Ambraseys, N. & Melville, C., 1982. *A History of Persian Earthquakes,* Cambridge University Press, UK.

Ambraseys, N., Moinfar, A. & Tchalenko, J., 1971. The Kamaveh (Northeast Iran) earthquake of 30 July 1970, *Ann. Geof.,* **24,** 475–495.

Ansari, F. & Bolourchi, M., 2003. Mud volcanoes of the east South Caspian Basin, Geological Survey of Iran.

Ashtari, M., Hatzfeld, D. & Kamalian, N., 2005. Microseismicity in the region of Tehran, *Tectonophysics,* **395,** 193–208.

Axen, G.J., Lam, P.S., Grove, M., Stockli, D.F. & Hassanzadeh, J., 2001. Exhumation of the west-central Alborz Mountains, Iran, Caspian subsidence, and collision-related tectonics, *Geology,* **29**(6), 559–562.

Berberian, M., 1981. Active faulting and tectonics of Iran, in *Zagros-Hindu Kush-Himalaya Geodynamic Evolution,* Chap. 3, pp. 33–69, eds Gupta, H. & Delany, F., Geodynamic Series, American Geophysical Union.

Berberian, M. & King, G., 1981. Towards a paleogeography and tectonic evolution of Iran, *Can. J. Earth Sci.,* **18**(2), 210–265.

Berberian, M. *et al.*, 2001. The 14 March 1998 Fandoqa earthquake (Mw 6.6) in Kerman province, S.E. Iran: re-rupture of the 1981 Sirch earthquake fault, triggering of slip on adjacent thrusts, and the active tectonics of the Gowk fault zone, *Geophys. J. Int.,* **146,** 371–398.

Bondár, I., Myers, S., Engdahl, E.R. & Bergman, E.A., 2004. Epicenter accuracy based on seismic network criteria, *Geophys. J. Int.,* **156,** 483–496.

Boyer, S. & Elliott, D., 1982. Thrust systems, *Am. Assoc. Petrol. Geol. Bull.,* **66**(9), 1196–1230.

Brunet, M.-F., Korotaev, M., Ershov, A. & Nikishin, A., 2003. The South Caspian Basin: a review of its evolution from subsidence modelling, *Sediment. Geol.,* **156**(1–4), 119–148.

Chapple, W. & Forsyth, D., 1979. Earthquakes and the bending of plates at trenches, *J. geophys. Res.,* **84,** 6729–6749.

Copley, A. & Jackson, J., 2006. Active tectonics of the Turkish-Iranian Plateau, *Tectonics,* **25**(TC6006), 1–19.

Devlin, W., Cogswell, J., Gaskins, G., Isaksen, G., Pitcher, D., Puls, D., Stanley, K. & Wall, G., 1999. South Caspian Basin: young, cool, and full of promise, *GSA Today,* **9**(7), 1–9.

Djamour, Y. *et al.*, 2010. GPS and gravity constraints on continental deformation in the Alborz mountain range, Iran, *Geophys. J. Int.,* **183,** 1287–1301.

Engdahl, E., van der Hilst, R. & Buland, R., 1998. Global teleseismic earthquake relocation with improved travel times and procedures for depth determination, *Bull. seism. Soc. Am.,* **88**(3), 722–743.

Engdahl, E., Jackson, J., Myers, S., Bergman, E. & Priestley, K., 2006. Relocation and assessment of seismicity in the Iran region, *Geophys. J. Int.,* **167,** 761–788.

Fattahi, M., Walker, R., Hollingsworth, J., Bahroudi, A., Nazari, H., Talebian, M., Armitage, S. & Stokes, S., 2006. Holocene slip-rate on the Sabzevar thrust fault, NE Iran, determined using optically stimulated luminescence (OSL), *Earth planet. Sci. Lett.,* **245**(3–4), 673–684.

Havskov, J. & Ottemöller, L., 2005. Seisan: the earthquake analysis software, version 8.1.

Hinds, D.J., Simmons, M.D., Allen, M.B. & Aliyeva, E., 2007. Architecture variability in the Pereriva and Balakhany suites of the neogene productive series, Azerbaijan: implications for reservoir quality, in *Oil and Gas of the Greater Caspian Area: AAPG Studies in Geology,* Vol. 55, pp. 87–107, eds Yilmaz, P.O. & Isaksen, G.H., American Association of Petroleum Geologists, Tulsa, OK.

Hollingsworth, J., Jackson, J., Walker, R., Gheitanchi, M. & Bolourchi, M., 2006. Strike-slip faulting, rotation, and along-strike elongation in the Kopeh Dagh mountains, NE Iran, *Geophys. J. Int.,* **166,** 1161–1177.

Hollingsworth, J., Jackson, J., Walker, R. & Nazari, H., 2008. Extrusion tectonics and subduction in the eastern South Caspian region since 10 Ma, *Geology,* **36**(10), 763–766.

Hollingsworth, J., Fattahi, M., Walker, R., Talebian, M., Bahroudi, A., Bolourchi, M., Jackson, J. & Copley, A., 2010a. Oroclinal bending, distributed thrust and strike-slip faulting, and the accommodation of Arabia-Eurasia convergence in NE Iran since the Oligocene, *Geophys. J. Int.,* **181,** 1214–1246.

Hollingsworth, J. *et al.*, 2010b. Active tectonics of the East Alborz mountains, NE Iran; rupture of the left-lateral Astaneh fault system during the great 856AD Qumis earthquake, *J. geophys. Res.,* **115,** B12313, doi:10.1029/2009JB007185.

Jackson, J., 2002. Strength of the continental lithosphere: time to abandon the jelly sandwich?, *GSA Today,* **12,** 4–10.

Jackson, J. & Fitch, T., 1979. Seismotectonic implications of relocated aftershock sequences in Iran and Turkey, *Geophys. J. R. astr. Soc.,* **57,** 209–229.

Jackson, J. & McKenzie, D., 1984. Active tectonics of the Alpine-Himalayan Belt between western Turkey and Pakistan, *Geophys. J. R. astr. Soc.,* **77**(1), 185–264.

Jackson, J., Haines, J. & Holt, W., 1995. The accommodation of Arabia–Eurasia plate convergence in Iran, *J. geophys. Res.,* **100**(B8), 15 205–15 219.

Jackson, J., Priestley, K., Allen, M. & Berberian, M., 2002. Active tectonics of the South Caspian Basin, *Geophys. J. Int.,* **148,** 214–245.

Javidfakhr, B., Bellier, O., Shabanian, E., Siame, L., Léanni, L., Bourlès, D. & Ahmadian, S., 2011. Fault kinematics and active tectonics at the southeastern boundary of the eastern Alborz (Abr and Khij fault zones): geodynamic implications for NNE Iran, *J. Geodyn.,* **52,** 290–303.

Kadinsky-Cade, K., Barazangi, M., Oliver, J. & Isacks, B., 1981. Lateral variations of high-frequency seismic wave propagations at regional distances across the Turkish and Iranian plateaus, *J. geophs. Res.,* **86,** 9377–9396.

Kennett, B. & Enghdal, E., 1991. Traveltimes for global earthquake location and phase identification, *Geophys. J. Int.,* **105,** 429–465.

Kissling, E., 1988. Geotomography with local earthquake data, *Rev. Geophys.,* **26,** 659–698.

Knapp, C., Knapp, J. & Connor, J., 2004. Crustal-scale structure of the South Caspian Basin revealed by deep seismic reflection profiling, *Mar. Petrol. Geol.,* **21,** 1073–1081.

Kopf, A., Klaeschen, D. & Mascle, J., 2001. Extreme effciency of mud volcanism in dewatering accretionary prisms, *Earth planet. Sci. Lett.,* **189,** 295–313.

Lee, W. & Lahr, J., 1972. HYPO71 (Revised), A computer program for determining hypocenters, magnitude and first motion pattern of local earthquakes, U.S. Geological Survey Open File Report, pp. 75–311.

Maggi, A., Priestley, K. & Jackson, J., 2002. Focal depths of moderate and large size earthquakes in Iran, *J. Seismol. Earthq. Eng.,* **4**(2–3), 1–10.

Maggi, M., Jackson, J., McKenzie, D. & Priestley, K., 2000. Earthquake focal depths, effective elastic thickness, and the strength of the continental lithosphere, *Geology,* **28**(6), 495–498.

Mangino, S. & Priestley, K., 1998. The crustal structure of the southern Caspian region, *Geophys. J. Int.,* **133,** 630–648.

Masson, F., Anvari, M., Djamour, Y., Walpersdorf, A., Tavakoli, F., Daignières, M., Nankali, H. & van Gorp, S., 2007. Large-scale velocity field and strain tensor in Iran inferred from GPS measurements: new insight for the present-day deformation pattern within NE Iran, *Geophys. J. Int.,* **170,** 436–440.

McCaffrey, R., 1991. Slip vectors and stretching of the Sumatran fore arc, *Geology,* **19**(9), 881–884.

McCaffrey, R. & Abers, J., 1988. SYN3: a program for inversion of teleseismic body wave form on microcomputers, Technical Report, Air Force Geophysical Laboratory, AFGL-TR 88-0099, Hanscomb Air Force Base, Massachusetts.

McCaffrey, R. & Nábělek, J., 1987. Earthquakes, gravity, and the origin of the Bali Basin: an example of a nascent continental fold-and-thrust belt, *Geophys. J. Int.,* **92,** 441–460.

Molnar, P. & Lyon-Caen, H., 1989. Fault plane solutions of earthquakes and active tectonics of the Tibetan Plateau and its margin, *Geophys. J. Int.,* **99,** 123–153.

Nábělek, J., 1984. Determination of earthquake source parameters from inversion of body waves, *PhD thesis,* MIT, Cambridge, Massachusetts.

Nemati, M., Hatzfeld, D., Gheitanchi, M., Sadidkhouy, A., Mirzaei, N. & Moradi, A., 2010. Investigation of Seismicity of the Astaneh Fault in the Eastern Alborz, *J. Earth Space Phys.,* **37**(2), 1–16.

Nemati, M., Hatzfeld, D., Gheitanchi, M., Sadidkhouy, A. & Mirzaei, N., 2011. Microseismicity of the Astane-Firouzkuh faults, east Alborz, Iran, Tectonophysics, *Tectonophysics,* **506**(1–4), 11–21.

Nissen, E., Tatar, M., Jackson, J. & Allen, M., 2011. New views on earthquake faulting in the Zagros fold-and-thrust belt of Iran, *Geophys. J. Int.,* **186,** 928–944.

Priestley, K., Baker, C. & Jackson, J., 1994. Implications of earthquake focal mechanism data for the active tectonics of the South Caspian Basin and surrounding regions, *Geophys. J. Int.,* **118**(1), 111–141.

Radjaee, A., Rham, D., Mokhtari, M., Tatar, M., Priestley, K. & Hatzfeld, D., 2010. Variation of Moho depth in the central part of the Alborz Mountains, northern Iran, *Geophys. J. Int.,* **181,** 173–184.

Raven, K., 2005. The nature of 'oceanic' basins trapped within the Alpine-Himalayan Belt, and their relationship to Tethys, *PhD thesis,* University of Cambridge.

Ritz, J.-F., Nazari, H., Ghassemi, A., Salamati, R., Shafei, A., Solaymani, S. & Vernant, P., 2006. Active transtension inside central Alborz: a new insight into northern Iran-southern Caspian geodynamics, *Geology,* **34**(6), 477–480.

Rizza, M., Mahan, S., Ritz, J.-F., Nazari, H., Hollingsworth, J. & Salamati, R., 2011. Using luminescence dating from coarse matrix material to estimate fault slip-rate in arid domain: example of the Astaneh Fault (Iran), *Quater. Geochronol.,* **6**(3–4), 390–406.

Shabanian, E., Bellier, O., Siame, L., Arnaud, N., Abbassi, M. & Cochemé, J., 2009a. New tectonic configuration in NE Iran: active strike-slip faulting between the Kopeh Dagh and Binalud mountains, *Tectonics,* **28,** TC5002, doi:10.1029/2008TC002444.

Shabanian, E., Siame, L., Bellier, O., Benedetti, L. & Abbassi, M., 2009b. Quaternary slip rates along the northeast boundary of the Arabia-Eurasia collision zone (Kopeh Dagh Mountains, north-east Iran), *Geophys. J. Int.,* **178,** 1055–1077.

Shabanian, E., Bellier, O., Abbassi, M., Siame, L. & Farbod, Y., 2010. Plio-Quaternary stress states in NE Iran: Kopeh Dagh and Allah Dagh-Binalud mountain ranges, *Tectonophysics,* **480**(1–4), 280–304.

Shad Manaman, N., Shomali, H. & Koyi, H., 2011. New constraints on upper-mantle S-velocity structure and crustal thickness of the Iranian plateau using partitioned waveform inversion, *Geophys. J. Int.,* **184**(1), 247–267.

Sloan, R., Jackson, J., McKenzie, D. & Priestley, K., 2011. Earthquake depth distribution in central Asia, and their relations with lithosphere thickness, shortening and extension, *Geophys. J. Int.,* **185**(1), 1–29.

Sodoudi, F., Yuan, X., Kind, R., Heit, B. & Sadidkhouy, A., 2009. Evidence for a missing crustal root and a thin lithosphere beneath the Central, *Geophys. J. Int.,* **177,** 733–742.

Stewart, S. & Davies, R., 2006. Structure and emplacement of mud volcano systems in the South Caspian Basin, *Am. Assoc. Petrol. Geol.,* **90**(5), 771–786.

Stöcklin, J., 1974. Possible ancient continental margins in Iran, in *Geology of Continental Margins,* pp. 873–877, eds Burke, C. & Drake, C., Springer-Verlag, New York.

Talebian, M. & Jackson, J., 2004. A reappraisal of earthquake focal mechanisms and active shortening in the Zagros mountains of Iran, *Geophys. J. Int.,* **156**(3), 506–526.

Talebian, M. *et al.*, 2006. The Dahuiyeh (Zarand) earthquake of 2005 February 22 in central Iran: reactivation of an intramountain reverse fault, *Geophys. J. Int.,* **164**(1), 137–148.

Tatar, M., Jackson, J., Hatzfeld, D. & Bergman, E., 2007. The 2004 May 28 Baladeh earthquake (Mw 6.2) in the Alborz, Iran: overthrusting the South Caspian Basin margin, partitioning of oblique convergence and the seismic hazard of Tehran, *Geophys. J. Int.,* **170,** 249–261.

Taymaz, T., Jackson, J. & McKenzie, D., 1991. Active tectonics of the north and central Aegean, *Sea, Geophys. J. Int.* **106,** 433–490.

Tchalenko, J.S., 1975. Seismicity and structure of the Kopet Dagh (Iran, USSR), *Phil. Trans. R. Soc. Lond. A.,* **278**(1275), 1–28.

Vernant, P. *et al.*, 2004a. Deciphering oblique shortening of central Alborz in Iran using geodetic data, *Earth planet. Sci. Lett.,* **223,** 177–185.

Vernant, P. *et al.*, 2004b. Present-day crustal deformation and plate kinematics in the Middle East constrained by GPS measurements in Iran and northern Oman, *Geophys. J. Int.,* **157**(1), 381–398.

Walker, R., 2003. Active faulting and tectonics of eastern Iran, *PhD thesis,* University of Cambridge.

Walker, R. & Jackson, J., 2004. Active tectonics and late Cenozoic strain distribution in central and eastern Iran, *Tectonics,* **23,** TC5010, doi:10.1029/2003TC001529.

Walpersdorf, A. *et al.*, 2006. Difference in the GPS deformation pattern of north and central zagros (Iran), *Geophys. J. Int.,* **167**(3), 1077–1088.

Wellman, H.W., 1966. Active wrench faults of Iran, Afghanistan, and Pakistan, *Geol. Rund.,* **55,** 716–735.

Wessel, P. & Smith, W. H.F., 1998. New, improved version of Generic Mapping Tools released, *EOS, Trans. Am. geophys. Un.,* **79**(47) 579, doi:10.1029/98EO00426.

Yusifov, M. & Rabinowitz, P., 2004. Classification of mud volcanoes in the South Caspian Basin, offshore Azerbaijan, *Mar. Petrol. Geol.,* **21**(8), 965–975.

Zanchi, A., Berra, F., Mattei, M., Ghassemi, M. & Sabouri, J., 2006. Inversion tectonics in central Alborz, Iran, *J. Struct. Geol.,* **28,** 2023–2037.

Zhao, L. & Helmberger, D., 1994. Source estimation from broadband regional seismograms, *Bull. seism. Soc. Am.,* **84**(1), 91–104.

Zhu, L. & Helmberger, D., 1996. Advancement in source estimation techniques using broadband regional seismograms, *Bull. seism. Soc. Am.,* **86,** 1634–1641.

Zwick, P., McCaffrey, R. & Abers, G., 1994. MT5 Program, IASPEI Software Library, 4.

APPENDIX

The distribution of first motions and the nodal planes for each earthquake is shown in Fig. A1.

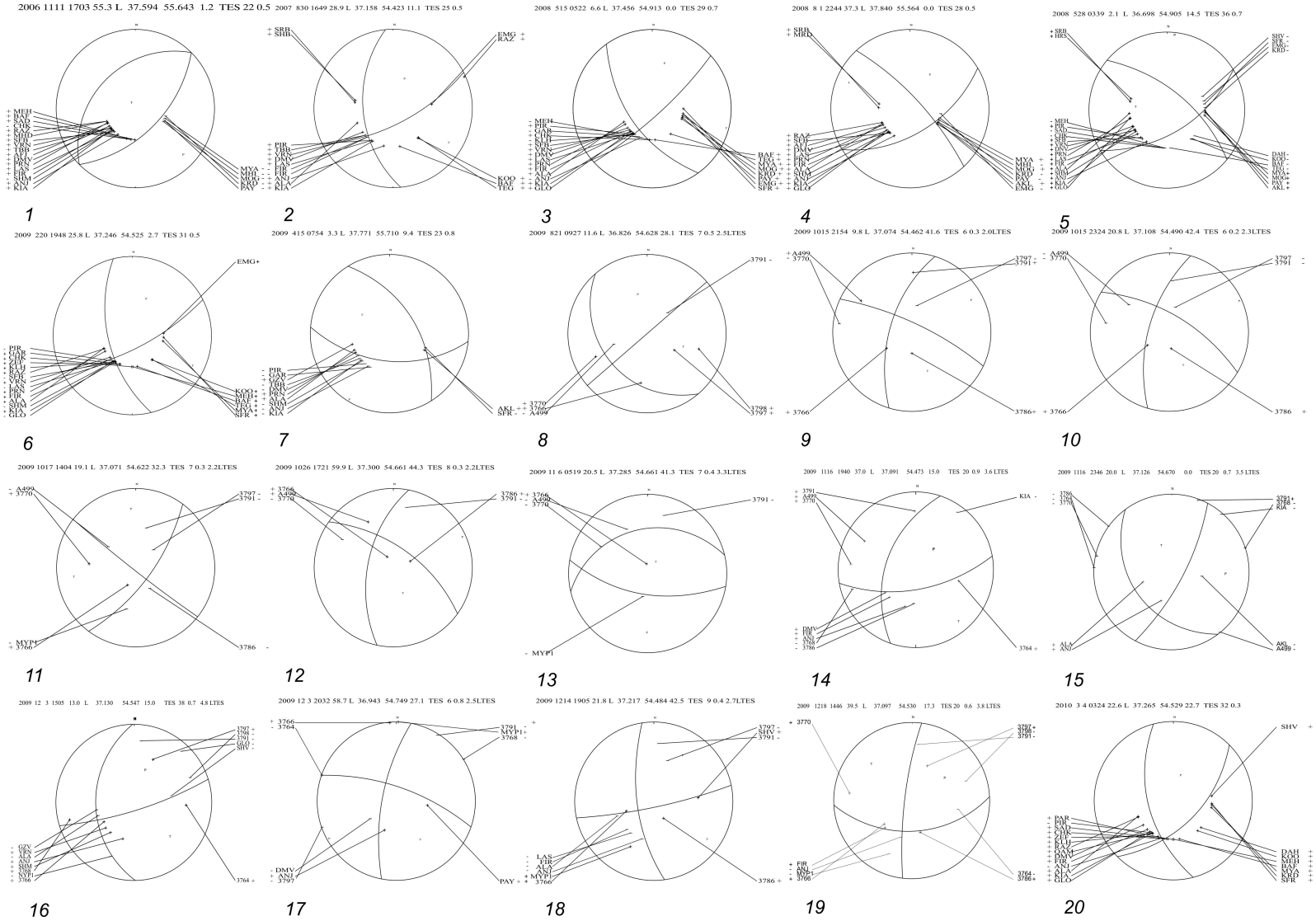

Figure A1. Focal meachanisms showing the distribution of first motions and the nodal planes for micro-earthquakes 1–20. Each plot is shown in a stereographic projection.